Dalton Transactions

Accepted Manuscript

ROYAL SOCIETY OF CHEMISTRY

www.rsc.org/dalton

Synthesis and Reactivity of Taddol-Based Chiral Fe(II) PNP Pincer Complexes - Solution Equilibria between κ^2*P,N*- and κ^3*P,N,P*-Bound PNP Pincer Ligands

Christian Holzhacker,[a] Berthold Stöger,[b] Maria Deus Carvalho,[c] Liliana P. Ferreira,[d,e] Ernst Pittenauer,[b] Günter Allmaier,[b] Luis F. Veiros,[f] Sara Realista,[c] Adrià Gil,[c] Maria José Calhorda,[c] Danny Müller,[a] and Karl Kirchner*,[a]

Abstract

Treatment of anhydrous FeX_2 (X = Cl, Br) with 1 equiv of the asymmetric chiral PNP pincer ligands PNP-R,TAD (R = *i*Pr, *t*Bu) with an *R,R*-TADDOL (TAD) moiety afforded complexes of the general formula [Fe(PNP)X_2]. In the solid state these complexes adopt a tetrahedral geometry with the PNP ligand coordinated in κ^2*P,N*-fashion, as shown by X-ray crystallography and Mössbauer spectroscopy. Magnetization studies led to a magnetic moment very close to 4.9 μ_B reflecting the expected four unpaired d-electrons (quintet ground state). In solution there are equilibria between [Fe(κ^3*P,N,P*-PNP-R,TAD)X_2] and [Fe(κ^2*P,N*-PNP-R,TAD)X_2] complexes, *i.e.*, the PNP-R,TAD ligand is hemilabile. At -50°C these equilibria are slow and signals of the non-coordinated P-TAD arm of the κ^2*P,N*-PNP-R,TAD ligand can be detected by $^{31}P\{^1H\}$ NMR spectroscopy. Addition of BH_3 to a solution of [Fe(PNP-*i*Pr,TAD)Cl_2] leads to selective boronation of the pendant P-TAD arm shifting the equilibrium towards the four-coordinate complex [Fe(κ^2*P,N*-PNP-*i*Pr,TAD^{BH_3})Cl_2]. DFT calculations corroborate the existence of equilibria between four- and five-coordinated complexes. Addition of CO to [Fe(PNP-*i*Pr,TAD)X_2] in solution yields the diamagnetic octahedral complexes *trans*-[Fe(κ^3*P,N,P*-PNP-*i*Pr,TAD)(CO)X_2], which react further with Ag^+ salts in the presence of CO to give the cationic complexes *trans*-[Fe(κ^3*P,N,P*-PNP-*i*Pr,TAD)$(CO)_2X]^+$. CO addition most likely takes place at the five coordinate complex [Fe(κ^3*P,N,P*-PNP-*i*Pr,TAD)X_2]. The mechanism for the CO addition was also investigated by DFT and the most favorable path obtained corresponds to the rearrangement of the pincer ligand first from a κ^2*P,N*- to a κ^3*P,N,P*-coordination mode followed by CO coordination to [Fe(κ^3*P,N,P*-PNP-*i*Pr,TAD)X_2]. Complexes bearing *t*Bu substituents do not react with CO. Moreover, in the solid state none of the tetrahedral complexes are able to bind CO.

[a]Institute of Applied Synthetic Chemistry, Vienna University of Technology, Getreidemarkt 9, A-1060 Vienna, AUSTRIA

[b]Institute of Chemical Technologies and Analytics, Vienna University of Technology, Getreidemarkt 9, A-1060 Vienna, AUSTRIA

[c]Centro de Química e Bioquímica, Faculdade de Ciências, Universidade de Lisboa, 1749-016 Lisboa, PORTUGAL

[d]Biosystems and Integrative Sciences Institute, Faculdade de Ciências, Universidade de Lisboa, 1749-016 Lisboa, PORTUGAL

[e]Department of Physics, University of Coimbra, 3004-516 Coimbra, PORTUGAL

[f]Centro de Química Estrutural, Instituto Superior Técnico, Universidade de Lisboa, Av. Rovisco Pais No. 1, 1049-001 Lisboa.

Introduction

Neutral pyridine-based PNP pincer ligands are widely utilized in transition metal chemistry due to their combination of stability, activity and variability.[1] They typically enforce a *meridional* κ^3*P,N,P* coordination mode, provided that three coordination sites are accessible at the metal center. As iron PNP complexes are concerned, an important class of compounds are coordinatively unsaturated 16e high-spin complexes of the type [Fe(κ^3*P,N,P*-PNP)X_2] (X = Cl, Br) obtained from the reaction of Fe(II) halides with stoichiometric amounts of PNP ligands.[2,3,4]

We are currently focusing on the synthesis and reactivity of iron complexes containing PNP pincer ligands based on the 2,6-diaminopyridine scaffold.[5] In these ligands the aromatic pyridine ring and the phosphine moieties are linked via NH, N-alkyl, or N-aryl linkers. In the course of our studies we discovered that Fe(II) halides react with bulky PNP ligands such as N,N'-bis(di-*iso*-propylphosphino)-2,6-diaminopyridine (PNP-*i*Pr) and N,N'-bis(di-*tert*-butylphosphino)-2,6-diamino-pyridine (PNP-*t*Bu) to give the expected mono-chelated high-spin complexes [Fe(κ^3*P,N,*P-PNP-R)X_2] (**A**). In contrast, with smaller PNP ligands such as N,N'-bis(diphenylphosphino)-2,6-diaminopyridine (PNP-Ph) or N,N'-bis(diethylphosphino)-2,6-diaminopyridine (PNP-Et), *bis*-chelated octahedral Fe(II) complexes [Fe(κ^3*P,N,P*-R)(κ^2*P,N*-PNP-R)X]$^+$ (**B**)[6] were formed where the PNP pincer ligands are coordinated in κ^3*P,N,P*- and κ^2*P,N*-fashion (Scheme 1).

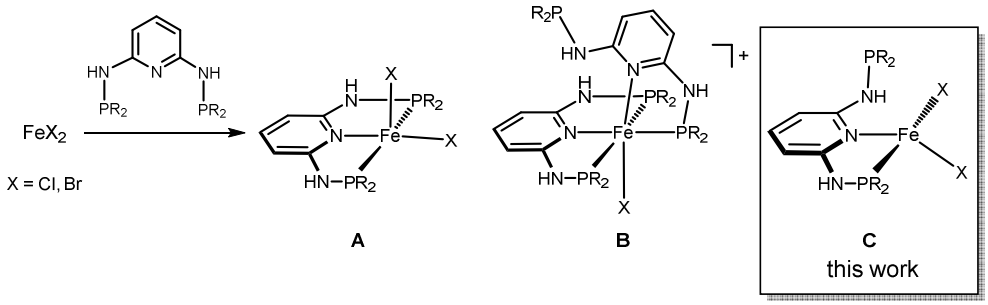

Scheme 1 Reactions of FeX_2 with PNP ligands yielding three types of complexes with κ^3*P,N,P*- and/or κ^2*P,N*-bound PNP ligands.

In continuation of our studies on iron PNP complexes, we report here on the synthesis and reactivity of chiral Fe(II) PNP pincer complexes based on *R,R*-TADDOL in combination with bulky *i*Pr and *t*Bu substituents to prevent the formation of **B**.[6] In the solid state these reactions afford complexes of the type [Fe(κ^2*P,N*-PNP-R,TAD)X_2] (R = *i*Pr, *t*Bu) (**C**) where the PNP ligand is coordinated in κ^2*P,N*-fashion (Scheme 1). In solution, complexes with κ^3*P,N,P*- and κ^2*P,N*-bound PNP ligands are in equilibrium with one another undergoing reversible dechelation and rechelation of the aminophosphine arm bearing the TAD moiety.

Results and Discussion

Ligand and Complex Synthesis. The synthesis of the new chiral PNP ligands PNP-*i*Pr,TAD (**2a**) and PNP-*t*Bu,TAD (**2b**) was achieved *via* a two-step procedure. First, addition of 1 equiv of PR_2Cl (R = *i*Pr, *t*Bu) to 2,6-diaminopyridine in the presence of base (NEt_3 or *n*BuLi) afforded the mono-phosphinated compounds **1a** and **1b**, respectively. Subsequent addition of 1 equiv of TAD-PCl in the presence of NEt_3 afforded then the desired PNP ligands **2a** and **2b** in 55 and 42% isolated overall yield (Scheme 2). The optically pure ligands were isolated as air stable solids and were characterized by ^{1}H, $^{13}C\{^{1}H\}$, and $^{31}P\{^{1}H\}$ NMR spectroscopy and HRMS.

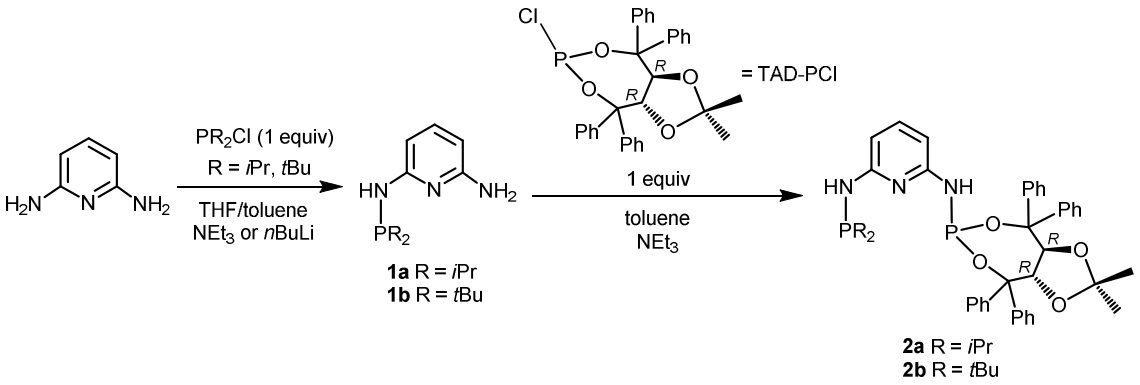

Scheme 2 Synthesis of chiral TADDOL-based PNP ligands

Treatment of anhydrous $FeCl_2$ with 1 equiv of the PNP ligands PNP-*i*Pr,TAD (**2a**) and PNP-*t*Bu,TAD (**2b**) in THF at room temperature afforded coordinatively unsaturated complexes of the general formula [Fe(PNP-*i*Pr,TAD)Cl_2] (**3a**) and [Fe(PNP-*t*Bu,TAD)Cl_2] (**4a**) in 79% isolated yields (Scheme 3). The analogous bromide complexes **3b** and **4b** were obtained in similar fashion by

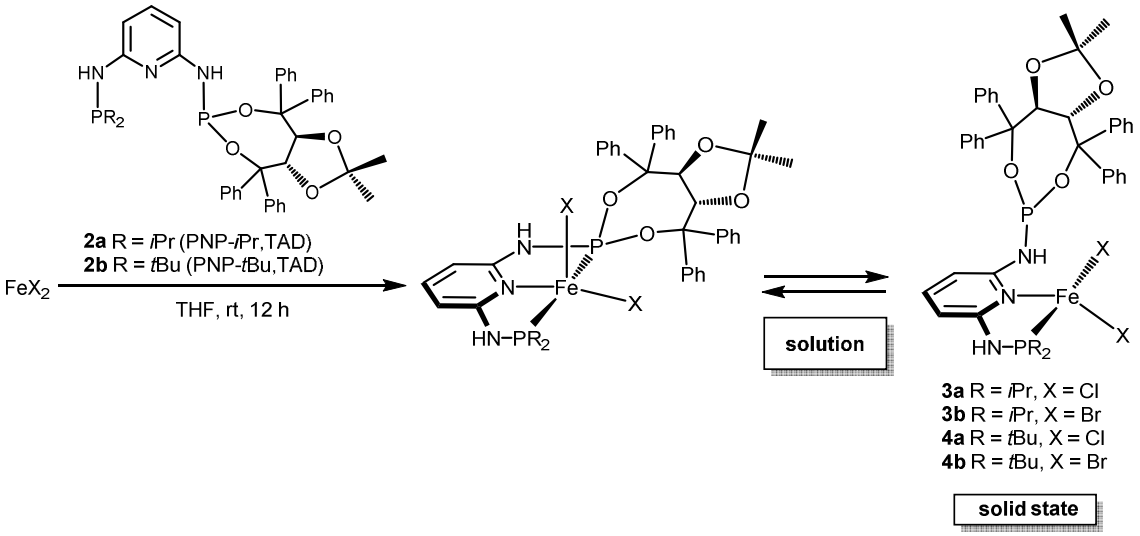

Scheme 3 Synthesis of [Fe(PNP-R,TAD)X_2] (**3**, **4**) – solution *vs* solid-state behavior

straightforward complexation of the respective free PNP ligands with anhydrous ferrous dibromide (89 and 89% yield). All complexes are thermally robust pale yellow solids that are air sensitive in the solid state and particularly in solution.

Solid State Studies. In the solid state, they were characterized by elemental analysis, SQUID and Mössbauer spectroscopy. In addition, the molecular structures of **3b** and **4a** were determined by X-ray crystallography. Structural views of **3b** and **4a** are depicted in Figures 1 and 2 with selected bond distances and angles given in the captions. Surprisingly, these complexes adopt a distorted tetrahedral geometry with the PNP ligands coordinated in κ^2*P,N*-fashion rather than in the typical *meridional* κ^3*P,N,P*-coordination mode. Such a coordination mode is unexpected and unusual for pyridine-based PNP pincer ligands in particular when taking into account that these complexes are coordinatively unsaturated 14e species.

Figures 1 and 2

The magnetic properties of **3a**, **3b**, **4a**, and **4b** were investigated by means of SQUID magnetometry and Mössbauer spectroscopy. Magnetic moments of μ_{eff} = 4.95(1), 4.98(1), 4.97(1), and 5.00(1)μ_B for **3a**, **3b**, **4a**, and **4b**, respectively, were derived from the temperature dependence of the inverse molar magnetic susceptibility, which was well described by a Curie law above 10 K (four unpaired electrons). These values are in good agreement with the effective magnetic moment of HS Fe(II) in the spin only approximation (4.9μ_B). The thermal variation of the inverse molar magnetic susceptibility and of χ_mT for all complexes is shown in Figure 3. Mössbauer spectroscopy of these complexes at 78 K showed isomer shifts (IS) of 0.76-0.79 mm/s and large quadrupole splittings (QS) in the range 2.93-3.22 mm/s (Table 1, Figure 4). All spectra confirm the exclusive presence of HS Fe(II), with higher isomer shifts and lower quadrupole splittings for the Cl complexes in comparison with the Br ones as was also previously observed and discussed for related Fe(II) complexes.[7] As can be seen from Table 1, the isomer shift and quadrupole splitting values are different from those observed for high-spin Fe(II) complexes with similar ligands but different geometries. When compared to compounds with square pyramidal coordination, it can be noticed that all tetrahedral complexes exhibit lower IS and higher QS values.[5c]

Figures 3 and 4

Solution Studies. While the solid state structures of complexes **3a**, **3b**, **4a**, and **4b** could be unequivocally established (**3b** and **4a** by X-ray crystallography), the situation in solution turned out to be more difficult due to the paramagnetic and complex nature of these compounds. It is not obvious whether these complexes are four- or five coordinate containing κ^2*P,N*- or κ^3*P,N,P*-bound PNP ligands, respectively, or whether both species are present and, if this is the case, whether these are in equilibrium with one another. Accordingly, several experiments were performed to provide information on the solution structure and behavior of **3a**, **3b**, **4a**, and **4b**.

ESI-MS studies (in the positive ion mode) of complexes **3a**, **3b**, **4a**, and **4b** in CH_3CN/CH_3OH (9:1) solutions revealed that these complexes remain largely intact and fragments of the sodiated complexes of [Fe(PNP-R,TAD)X_2] ([M+Na]$^+$) were observed at m/z 868.2, 886.1, 896.2, and 984.1, respectively. Further abundant fragments are [M-X]$^+$ (for **3a**, **4a**, **4b**), [M-X+CH_3OH]$^+$ (for **3a**, **4a**), and [M-X-HX+CH_3OH]$^+$ (for **4a**) revealing the high affinity of CH_3OH towards these Fe(II) complexes. A representative positive ion ESI full scan mass spectra of **3b** is depicted in Figure 5. In the inset, the isotopic pattern of the [M+Na]$^+$ ion is compared with the theoretical pattern, which turned out to correlate quite well.

Figure 5

All complexes display large paramagnetic shifted ^{1}H and ^{13}C{^{1}H} NMR solution spectra with broad and featureless signals which, due to the complexity of the PNP ligands, were not assignable and thus not informative. Interestingly, while at room temperature no ^{31}P{^{1}H} NMR signals could be detected, at -50°C complexes **3** and **4** exhibit a broad signal at about 126 ppm, assignable to the non-coordinated TAD arm of the κ^2*P,N*-bound PNP-R,TAD ligands based on the fact that the free ligands **2a** and **2b** give rise to signals at 134.6 and 132.4 ppm. This observation clearly points to an equilibrium between κ^2*P,N*- and κ^3*P,N,P*-bound species, *i.e.*, the PNP-R,TAD ligand is hemilabile, which is also supported by DFT calculations (*vide infra*). Related solution equilibria were proposed for the pincer complex [Fe(PONOP-*t*Bu)Cl_2] bearing the bulky *bis*-phosphinte PONOP-*t*Bu ligand.[8] Moreover, addition of BH_3·THF to a solution of **3a** in CD_2Cl_2 leads to boronation of the pendant TAD arm shifting the equilibrium towards the four-coordinate complex [Fe(κ^2*P,N*-PNP-*i*Pr,TAD^{BH_3})Cl_2] (**5**) (Scheme 4). ^{31}P{^{1}H} NMR spectra of these studies are shown in Figure 6. An ESI-MS study of **5** in CH_3CN/CH_2Cl_2 gave rise to largely intact fragments of the sodiated species [**5**+Na]$^+$ and [**5**-Cl]$^+$ observed at m/z 882.1 and 824.1.

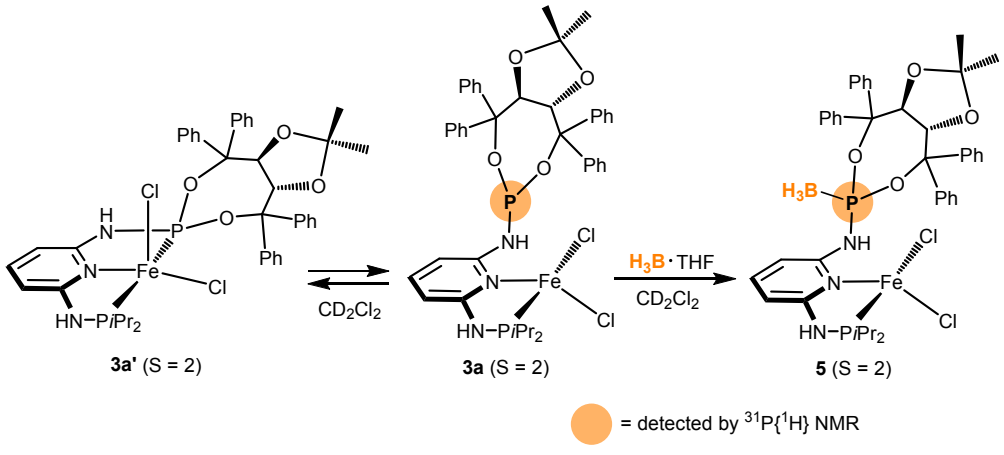

3a' (S = 2) **3a** (S = 2) **5** (S = 2)

Scheme 4 Solution equilibria and boronation of [Fe(κ^2*P,N*-PNP-*i*Pr,TAD)Cl_2] (**3a**) and [Fe(κ^3*P,N,P*-PNP-*i*Pr,TAD)Cl_2] (**3a'**) with BH_3·THF in CD_2Cl_2.

Figure 6

Reactivity towards CO. When CO was bubbled into acetone solutions of **3a** and **3b** for a few minutes, an immediate color change from pale yellow to violet and blue, respectively, was observed due the formation of *trans*-[Fe(κ^3*P,N,P*-PNP-*i*Pr/TAD)(CO)Cl_2] (**6a**) and *trans*-[Fe(κ^3*P,N,P*-PNP-*i*Pr/TAD)(CO)Br_2] (**6b**). (Scheme 5). Pure crystalline materials had to be obtained by diffusion of *n*-pentane into a THF solution of **6a** and **6b**, respectively, since evaporation of the solvent resulted in rapid CO loss and reformation of **3a** and **3b**. In the case of the bulkier *t*Bu complexes **4a** and **4b**, no CO addition was observed. The same behavior was found for [Fe(κ^3*P,N,P*-PNP-*t*Bu)X_2]. Noteworthy, in the solid state none of the tetrahedral complexes underwent CO addition, in contrast to the reactions of the five coordinate complexes [Fe(κ^3*P,N,P*-PNP-*i*Pr)X_2] reported previously.[9] Complexes **6a** and **6b** were fully characterized by ^{1}H, ^{13}C{^{1}H}, and ^{31}P{^{1}H} NMR and IR spectroscopy. The ^{31}P{^{1}H} NMR spectra give rise to two doublets centered at 154.0/125.0 and 161.6/125.2 ppm, respectively, with large J_{PP} coupling constants of 278 and 261 Hz which are consistent with a *trans*-P,P configuration (Figure 6, spectrum d). In the ^{13}C{^{1}H} NMR spectra the CO ligands exhibit a single low-intensity doublet of doublet resonance at 220.3 and 222.5 ppm. Complexes **6a** and **6b** give rise to one band at 1986 and 1980 cm^{-1} in the IR spectrum (*cf* 2143 cm^{-1} in free CO). For comparison, in *trans*-[Fe(κ^3*P,N,P*-PNP-*i*Pr)(CO)Cl_2] and *trans*-[Fe(κ^3*P,N,P*-PNP-*i*Pr)(CO)Br_2] the CO stretching frequency is observed at 1956 cm^{-1}, indicating that PNP-*i*Pr,TAD is a weaker donor than PNP-*i*Pr.[5c]

The solid state structure of **6b** could be determined by single-crystal X-ray diffraction. Crystals were grown under a CO atmosphere from a THF solution by diffusion of pentane. An ORTEP diagram is depicted in Figure 7 with selected bond distances given in the captions. This complex adopts a distorted octahedral geometry around the metal center with the bromide ligands being in *trans* position to one another. The PNP ligand is now coordinated to the iron center in the typical tridentate meridional κ^3*P,N,P* mode.

Figure 7

Heating solid samples of **6a** and **6b** leads to regeneration of complexes [Fe(κ^2*P,N*-PNP-*i*Pr,TAD)Cl_2] (**3a**) and [Fe(κ^2*P,N*-PNP-*i*Pr,TAD)Br_2] (**3b**). However, loss of CO is slow with about 80% conversion after 2h. The Mössbauer spectra of the complex **6b** before and after being partially decarbonylated (by heating at 100^{o}C for 1h and 2h under vacuum) are shown in Figure 8. The spectrum of **6b** is well fitted to a quadrupole doublet with IS = 0.23(1) mm/s and QS = 1.19(1) mm/s assignable to a typical low spin Fe(II) complex in a symmetric octahedral environment. The isomer shift decrease observed from **3b** to **6b** is explained by the HS-LS change induced by the reaction with CO. Accordingly, the decrease in the quadrupole splitting values is explained by the much less asymmetric environment of Fe(II) in six coordination (**6b**) than in four coordination (**3b**).

Figure 8

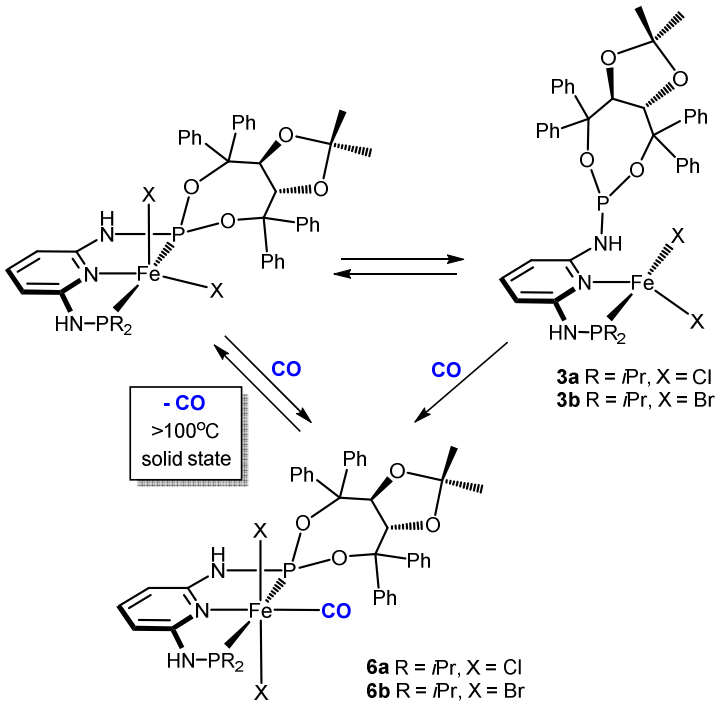

Scheme 5 Reaction of [Fe(PNP-*i*Pr,TAD)X_2] (**3a**,**b**) with CO in solution forming *trans*-[Fe(κ^3*P,N,P*-PNP-*i*Pr,TAD)(CO)X_2] (**6a**,**b**).

When compared with the hyperfine parameters of **6b** spectrum (Table 1), it can be deduced that 60% and 21% of this contribution remains unreacted in the 1h and 2h annealed samples, respectively. A second doublet appears in these partially decarbonylated samples, displaying hyperfine parameters of IS = 0.78(1) mm/s, QS = 3.07(2) mm/s and IS = 0.79(1) mm/s, QS = 3.15(1) mm/s, for the 1h and 2h annealed samples, respectively. As can be seen from Table 1, the isomer shift and quadrupole splitting values of [Fe(κ^2*P,N*-PNP-*i*Pr,TAD)X_2] complexes are different from those observed for high-spin Fe(II) complexes with similar ligands but different geometries. In particular, when compared to compounds with square pyramidal geometry, it can be noticed that all tetrahedral complexes exhibit lower IS and higher QS values.[5c] Therefore, the second doublet detected in the decarbonylated samples can be assigned to [Fe(κ^2*P,N*-PNP-*i*Pr,TAD)Br_2] (**3b**), indicating that at higher temperatures the CO release in the solid state does not induce the formation of the penta-coordinated [Fe(κ^3*P,N*-PNP-*i*Pr,TAD)Br_2] (**3b'**) complex.

The isomer shift and quadrupole splitting of complexes **3b, 3b'**and **6b** were calculated using a DFT approach, as 0.873 (**3b**), 0.972 (**3b'**), and 0.478 (**6b**) mm/s and 2.694 (**3b**), 2.652 (**3b'**), and 0.675 (**6b**) mm/s, respectively. Despite the small deviation, the trends are well reproduced. The isomer shift of **3b** is much higher than that of **6b**, as observed experimentally. The pentacoordinate complexes often display isomer shifts ~0.1 higher than the tetrahedral ones (see examples in Table 1), and our calculations also predict a similar difference (0.873 and 0.972 mm/s for **3b** and **3b'**,

respectively). These values suggest that the signal of a pentacoordinate species should have been detected if such a species were present in the solid state, supporting the experimental results described above.

Treatment of **6a** and **6b** with 1 equiv of $AgSbF_6$ in THF in the presence of CO at room temperature afforded selectively the cationic complexes *trans*-[Fe(κ^3*P,N,P*-PNP-*i*Pr,TAD)$(CO)_2X]^+$ (**7a**,**b**) in 80 and 81% isolated yields (Scheme 6). These complexes are thermally robust red solids that are air stable both in the solid state and in solution for several days. In the $^{13}C\{^1H\}$ NMR spectrum the two CO ligands are chemically and magnetically not equivalent thus giving rise to two low-intensity

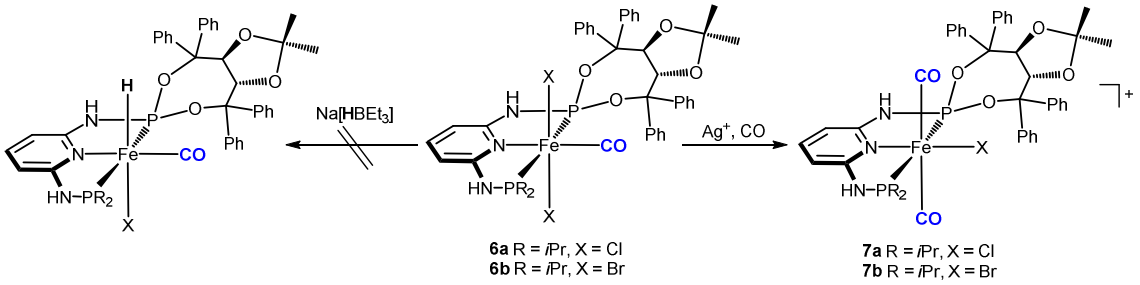

Scheme 6 Reaction of [Fe(κ^3*P,N,P*-PNP-*i*Pr,TAD)$(CO)X_2$] (**6a**,**b**) with CO in the presence of Ag^+ forming *trans*-[Fe(κ^3*P,N,P*-PNP-*i*Pr,TAD)$(CO)_2X]^+$ (**7a**,**b**) and attempted reaction with Na[$HBEt_3$].

doublet of doublet resonances centered at about 207 ppm. In the IR spectrum the CO ligands exhibit only one band at 2026 and 2021 cm^{-1} for the mutually *trans* CO ligands which can be assigned to the asymmetric CO stretching frequency. The symmetric CO stretching band is IR inactive and thus not observed.

Finally, since the hydride complex [Fe(κ^3*P,N,P*-PNP-*i*Pr)(CO)(H)Br] turned out to be an efficient hydrogenation catalyst for both ketones and aldehydes,[10] we have attempted to prepare chiral hydride complexes of the type [Fe(κ^3*P,N,P*-PNP-*i*Pr,TAD)(CO)(H)X] following an established procedure. However, treatment of **6a** or **6b** with Na[$HBEt_3$] lead to decomposition and the only tractable products which could be isolated were the free PNP ligands.

Computational Studies. The change in coordination of the PNP ligand from a κ^2*P,N* to a κ^3*P,N,P* mode was investigated by means of DFT calculations[11] (see Computational Details) using a model of complex **3b** (R = *i*Pr, X = Br) with a simplified TADDOL moiety (TAD'). In the model the phenyl groups were replaced by H-atoms for computational expediency. The energy profile for the rearrangement between the four-coordinated complex with a κ^2*P,N*-PNP ligand (**A**) and the penta-coordinated species with a κ^3*P,N,P*-PNP ligand (**C**) is shown in Scheme 7.

The mechanism for the coordination of the second P-atom in [Fe(PNP-*i*Pr,TAD')Br_2] comprises two steps. The first is re-orientation of the pendant arm of the PNP ligand in the reactant, with rotation along the C_{py}-N_{NH} bond. In the second step, the P-atom coordinates the metal. The overall process has an energy barrier of 9.8 kcal/mol (corresponding to $\mathbf{TS_{BC}}$) and indicates a facile process that should occur easily at room temperature. This is in agreement with ^{31}P NMR studies

(Figure 6). Since the five-coordinated isomer **C** is only 3.6 kcal/mol less stable than the initial complex **A**, the profile in Scheme 7 suggests that an equilibrium between the two forms may occur in solution. Importantly, the performance of the model used in the calculations was tested through the comparison of the stability difference obtained for the two isomers calculated with the real species, that is, with full

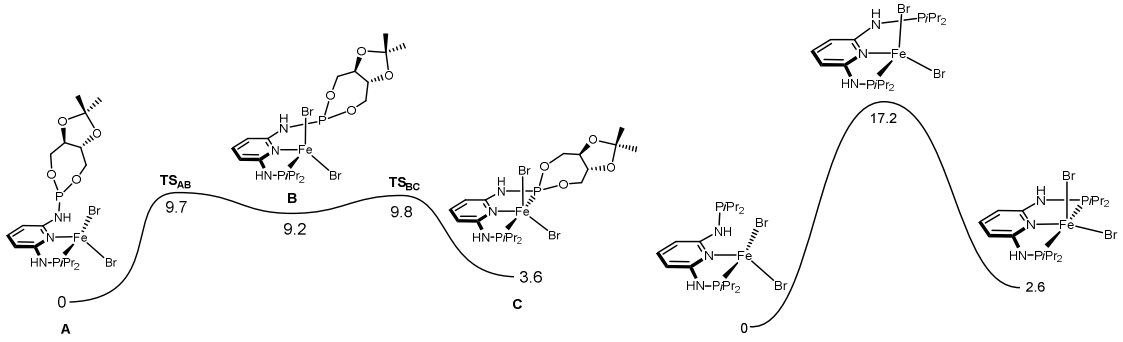

Scheme 7. Energy profile (kcal/mol) for the rearrangement between κ^2*P,N* and κ^3*P,N,P* in [Fe(PNP-*i*Pr,TAD')Br_2] and comparison with [Fe(PNP-*i*Pr)Br_2].

TADDOL fragments in the PNP ligands. The results indicate that the four-coordinated species is more stable than its five-coordinated counterpart by 2.8 kcal/mol, a value that is only 0.8 kcal/mol smaller than the one obtained with the simplified model and validates the use of that model in the calculations. For comparison, the equilibrium between [Fe(κ^3*P,N,P*-PNP-*i*Pr)Br_2] and [Fe(κ^2*P,N*-PNP-*i*Pr)Br_2] was also investigated (Scheme 7). This process proceeds via a single step but with a considerably higher barrier of 17.2 kcal/mol and agrees with the fact experimentally no [Fe(κ^2*P,N*-PNP-*i*Pr)Br_2] complex was detected as the was no BH_3 adduct formed. These results may also suggest that the hemilability of the PNP-R,TAD ligand is not due to steric but electronic reasons.

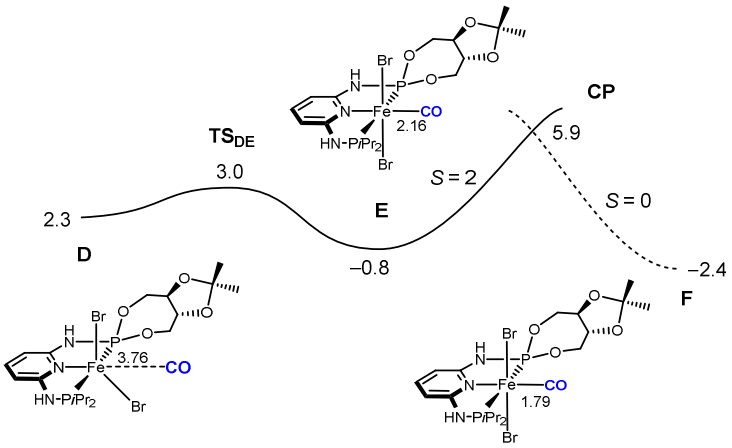

Scheme 8. Energy profile (kcal/mol) for the reaction of CO addition to [Fe(κ^3*P,N,P*-PNP-*i*Pr,TAD')Br_2]. The energy values are referred to **A**, and the Fe-C_{CO} distances (Å) are indicated. The full curve

corresponds to the *S* = 2 potential energy surface (PES), and the dashed curve corresponds to the *S* = 0 PES.

The energy profile calculated for CO addition to the five-coordinated complex [Fe(κ^3*P,N,P*-PNP-*i*Pr,TAD')Br_2] is represented in Scheme 8. The first step of the mechanism occurs in the spin quintet (*S* = 2) potential energy surface (PES). Starting point is the pair of reactants **D**, *i.e.,* the five-coordinated complex and one CO molecule. From **D** CO addition occurs in a single step going through a rather early transition state ($\mathbf{TS_{DE}}$) with a long Fe-C_{CO} bond distance (3.01 Å) indicating that CO coordination is only starting once that transition state is reached. In the resulting intermediate **E** CO coordination is established with a Fe-C_{CO} distance of 2.16 Å. This step is thermodynamically favorable (ΔE = -3.1 kcal/mol) and has a negligible barrier of 0.7 kcal/mol. Since the product of the reaction is the low spin (*S* = 0) CO adduct **F**, there must be a spin change from the quintet to the singlet spin PES in the last step of the mechanism. In other words, this is a "spin forbidden" or "non-adiabatic" reaction and, thus, the change between PES occurs through a minimum-energy crossing point (MECP). In the MECP both the geometry and the energy of the molecules are the same in the two PES. Once that point is reached along the reaction coordinate there is a given probability for the system to change spin state and hop from one spin state to the other, completing the "spin-forbidden" reaction. Accordingly, in the last step of the mechanism depicted in Scheme 7, the high spin CO complex, **E** (*S* = 2), changes to its low spin isomer, **F** (*S* = 0), through a crossing point (**CP**) that has an intermediate geometry between the two CO species. The moderate energy barrier associated with the spin exchange (6.7 kcal/mol) reflects the small geometry modifications associated with this step. The final product **F** is 2.4 kcal/mol more stable than the initial reagent, the four-coordinated species [Fe(κ^2*P,N*-PNP-*i*Pr,TAD')Br_2] (**A**).

From the two profiles it becomes clear that the most difficult process along the path is coordination of the second P-atom of the PNP ligand, rather than CO addition or spin change. In fact, the highest barrier along the entire mechanism is associated with $\mathbf{TS_{BC}}$, *i.e.*, the step corresponding to the coordination of the dangling P-atom, from **B** to **C** (see Scheme 6).

An alternative mechanism is CO addition to the four-coordinated complex [Fe(κ^2*P,N*-PNP-*i*Pr,TAD')Br_2] followed by a subsequent change in the coordination mode of the PNP ligand from κ^2*P,N* to κ^3*P,N,P* with coordination of the free P-atom. The energy profile for this process is depicted in Scheme 9.

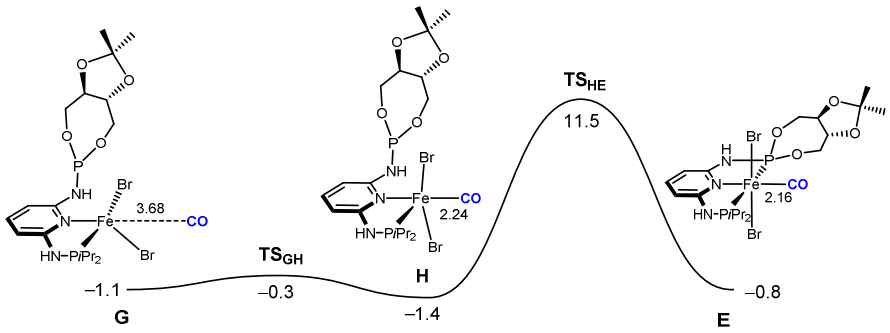

Scheme 9. Energy profile (kcal/mol) for the reaction of CO addition to [Fe(κ^2*P,N*-PNP-*i*Pr,TAD')Br_2] followed by exchange of the coordination of the pincer ligand from κ^2*P,N* to κ^3*P,N,P*. The energy values are referred to **A**, and the Fe-C_{CO} distances (Å) are indicated.

The mechanism starts with a pair of non-interacting reactants **G**, the CO molecule and the [Fe(κ^2*P,N*-PNP-*i*Pr,TAD')Br_2] complex. In the first step there is CO addition and formation of a five-coordinated CO complex **H** that maintains the PNP dangling arm existing in the initial complex. A rather long Fe-C_{CO} distance of 2.80 Å in the corresponding transition state (**TS_{GH}**) indicates that CO coordination is just beginning when **TS_{GH}** is reached along the reaction coordinate. This step occurs with a very small barrier of 0.8 kcal/mol and the intermediate **H** formed is only 0.3 kcal/mol more stable than the initial reagents. In the second step of the mechanism, from **H** to **E**, there is coordination of the P-atom of the PNP ligand, originating the high spin six-coordinated CO complex. Coordination of the P-atom in the CO species occurs in a single step, from **H** to **E**, through the transition state **TS_{HE}**. In **TS_{HE}**, formation of the new Fe–P bond is still far from complete, as indicated by a distance of 3.64 Å, which is 1.08 Å longer than the coordination distance in **E**. This step is practically thermoneutral (ΔE = 0.6 kcal/mol) and the corresponding barrier (12.9 kcal/mol) is the highest of that path.

In the first mechanism, coordination of the loose P-atom of the pincer ligand, with the corresponding change from κ^2*P,N* to κ^3*P,N,P* occurs first and it is followed by CO addition. This path corresponds to the profiles represented in Schemes 7 and 8, and its highest barrier is 9.8 kcal/mol. In the second path, the order of the processes is reversed. First there is addition of CO to the four-coordinated complex with κ^2*P,N*-PNP, and only then occurs coordination of the free P-atom. The highest barrier obtained for this case, associated with the P-coordination step (**TS_{HE}** in Scheme 9), is 12.9 kcal/mol and slightly higher by 3.1 kcal/mol than the barrier associated with the first mechanism. Therefore, the first mechanism should be slightly favored.

This trend is supported by the fact that, despite their relatively low formal electron count, the related four coordinate complexes [Fe(κ^2*P,N*-PN-*i*Pr)X_2] (PN-*i*Pr = *N*-diisopropylphosphino-2-aminopyridine) did not react with CO at ambient temperature,[12] while pentacoordinate complexes [Fe(κ^3*P,N,P*-PNP-*i*Pr)X_2] readily added CO to give octahedral complexes of the type [Fe(κ^3*P,N,P*-PNP-*i*Pr)(CO)X_2]. In general, the outcome of a CO addition to high spin iron(II) complexes depends on the geometry and coordination number, the key factor being the overall ligand field of the ensemble of ligands in the reactant. Accordingly, the lower the coordination number the less likely CO addition will take place and reactions will be disfavored.[13]

Conclusions

We have prepared several Fe(II) complexes of the general formula [Fe(PNP-R,TAD)X_2] (R = *i*Pr, *t*Bu; X = Cl, Br) bearing asymmetric chiral pincer ligands based on *R,R*-TADDOL (TAD). In the solid state, as shown by X-ray crystallography, Mössbauer and IR spectroscopy, these complexes adopt a tetrahedral geometry with the PNP ligand coordinated in κ^2*P,N*-fashion with the TAD arm being not coordinated. All complexes are paramagnetic with a quintet ground state. In solution there are equilibria between [Fe(κ^3*P,N,P*-PNP-R,TAD)X_2] and [Fe(κ^2*P,N*-PNP-R,TAD)X_2] complexes and the

PNP-R,TAD ligand is hemilabile. DFT calculations indicate that the rearrangement of the pincer ligands is an accessible process and, thus, equilibria between the four-coordinated species and their five-coordinated counterparts is expected to occur. Addition of CO to [Fe(PNP-*i*Pr,TAD)X_2] in solution yields the diamagnetic octahedral complexes *trans*-[Fe(κ^3*P,N,P*-PNP-*i*Pr,TAD)(CO)X_2], which react further with Ag^+ salts in the presence of CO to give the cationic complexes *trans*-[Fe(κ^3*P,N,P*-PNP-*i*Pr,TAD)$(CO)_2X]^+$. Complexes bearing *t*Bu substituents do not react with CO. Moreover, in the solid state none of the tetrahedral complexes are able to bind CO. Addition of CO most likely takes place at the five coordinate complex [Fe(κ^3*P,N,P*-PNP-*i*Pr,TAD)X_2]. The mechanism for this process was investigated by DFT and the most favorable path obtained corresponds to the rearrangement of the pincer ligand first from a κ^2*P,N*- to a κ^3*P,N,P*-coordination mode followed by CO coordination to [Fe(κ^3*P,N,P*-PNP-*i*Pr,TAD)X_2]. The alternative path with a reversed order of the two processes is competitive and the possible occurrence of both at the same time may not be discarded. Heating solid samples of *trans*-[Fe(κ^3*P,N,P*-PNP-*i*Pr,TAD)$(CO)_2X]^+$ at 100°C under vacuum leads to regeneration of complex [Fe(κ^2*P,N*-PNP-*i*Pr,TAD)X_2]. Loss of CO is slow with about 80% conversion after 2h. Mössbauer measurements show no evidence for the formation of [Fe(κ^3*P,N,P*-PNP-*i*Pr,TAD)X_2] suggesting that at higher temperatures the PNP ligands are flexible enough to change their coordination modes also in the solid state.

Experimental Section

General. All manipulations were performed under an inert atmosphere of argon by using Schlenk techniques or in a MBraun inert-gas glovebox. The solvents were purified according to standard procedures.[14] The deuterated solvents were purchased from Aldrich and dried over 4 Å molecular sieves. TAD-PCl was prepared according to the literature.[15] ^{1}H, ^{13}C{^{1}H}, and ^{31}P{^{1}H} NMR spectra were recorded on Bruker AVANCE-250, AVANCE-300 DPX, and AVANCE-400 spectrometers. ^{1}H and ^{13}C{^{1}H} NMR spectra were referenced internally to residual protio-solvent, and solvent resonances, respectively, and are reported relative to tetramethylsilane (δ = 0 ppm). ^{31}P{^{1}H} NMR spectra were referenced externally to H_3PO_4 (85%) (δ = 0 ppm). ^{11}B NMR spectra were referenced externally to $BF_3{\cdot}Et_2O$.

Magnetization measurements as a function of temperature were performed on powder samples using a SQUID magnetometer (Quantum Design MPMS). The curves were obtained under 0.1 T, for temperatures ranging from 10 to 300 K. The molar susceptibility values (χ_m) were corrected for diamagnetism of the constituent atoms using Pascal constants.

The ^{57}Fe Mössbauer spectra were recorded in transmission mode at 78 K using a conventional constant-acceleration spectrometer and a 50 mCi ^{57}Co source in a Rh matrix. The measurements were performed using a liquid nitrogen flow cryostat with a temperature stability of $\pm$0.5 K. The velocity scale was calibrated using an α-Fe foil. The spectra were fitted to Lorentzian lines using the WinNormos software program, and the isomer shifts reported are relative to metallic α-Fe at room temperature.

Mass spectrometric measurements were performed on an Esquire 3000^{plus} 3D-quadrupole ion trap mass spectrometer (Bruker Daltonics, Bremen, Germany) in positive-ion mode by means of electrospray ionization (ESI). Mass calibration was done with a commercial mixture of perfluorinated trialkyltriazines (ES Tuning Mix, Agilent Technologies, Santa Clara, CA, USA). All analytes were dissolved in a mixture of CH_3CN and CH_3OH "hypergrade for LC-MS Lichrosolv" quality (Merck, Darmstadt, Germany) to form a concentration of roughly 1 mg/mL. Direct infusion experiments were carried out using a Cole Parmer model 74900 syringe pump (Cole Parmer Instruments, Vernon Hills, IL, USA) at a flow rate of 2 μL/min. Full scans were measured in the range m/z 100-1100 with the target mass set to m/z 1000. All mass calculations are based on the lowest mass (i.e. most abundant) iron isotope (^{56}Fe-isotope). Mass spectra were averaged during data acquisition time of 1 to 2 min and one analytical scan consisted of five successive micro scans resulting in 50 and 100 analytical scans, respectively, for the final full scan mass spectrum.

Synthesis. [PN/NH$_2$-*i*Pr] (1a). 2,6-Diaminopyridine (6.87 g, 62.95 mmol) was suspended with NEt_3 (8.7 mL, 62.95 mmol) in 1:1 mixture of THF/toluol (150 mL) and cooled to 0°C. P*i*Pr$_2$Cl (4.80 g, 31.47 mmol) was added slowly via syringe. The resulting mixture was allowed to reach room temperature and was stirred overnight at 80°C. The solution was extracted at room temperature with 50 mL of a saturated $NaHCO_3$ solution, followed by extraction with 50 mL of brine. The combined organic phases were dried over Na_2SO_4, filtered and the solvent was removed under vacuum. The product was purified *via* flash chromatography (ethyl acetate/petrol ether 2:1 → ethyl acetate) and isolated as white crystals. Yield: 4.32 g (61%). ^{1}H NMR (δ, $CDCl_3$, 20°C): 7.25 (t, $^3J_{HH}$ = 7.9 Hz, 1H, py^4), 6.46 (d, $^3J_{HH}$ = 7.9 Hz, 1H, py^3), 5.90 (d, $^3J_{HH}$ = 7.7 Hz, 1H, py^5), 4.40 (d, $^2J_{PH}$ = 10.7 Hz, 1H, N*H*), 4.18 (s, 2H, NH_2), 1.77 (m, 2H, C*H*(CH$_3$)$_2$), 1.07 (m, 12H, CH(CH_3)$_2$). ^{13}C{^{1}H} NMR (δ, $CDCl_3$, 20°C): 159.86 (d, $^2J_{CP}$ = 20.3 Hz, py^2), 157.28 (py^6), 139.42 (d, $^4J_{CP}$ = 2.1 Hz, py^4), 97.99 (d, $^3J_{CP}$ = 18.3 Hz, py^3), 97.99 (py^5), 26.37 (d, $^1J_{CP}$ = 11.2 Hz, *C*H(CH$_3$)$_2$), 18.66 (d, $^2J_{CP}$ = 19.7 Hz, CH(*C*H$_3$)$_2$), 17.05 (d, $^2J_{CP}$ = 7.8 Hz, CH(*C*H$_3$)$_2$). ^{31}P{^{1}H} NMR (δ, $CDCl_3$, 20°C): 47.4. MS (ESI-HRMS, CH_3CN) (m/z): [M+H]$^+$ ($C_{11}H_{21}N_3P$) calcd 226.1468. Found 226.1453.

[PN/NH$_2$-*t*Bu] (1b). 2,6-Diaminopyridine (5.17 g, 47.37 mmol) was dissolved in THF (120 mL) and cooled to -10°C. *n*BuLi (9.6 mL, 24.16 mmol, 2.5 M) was added slowly via syringe, whereupon the solution turned dark red and a precipitate was formed. The mixture was allowed to warm up to room temperature and was stirred for 3 h. After cooling to -10°C P*t*Bu$_2$Cl (4.28 g, 23.69 mmol) was added and the solution was then warmed to 80°C and stirred overnight. Workup was performed in the same way as for compound **1a**. The product was isolated as a pale yellow powder. Yield: 2.70 g (45%). ^{1}H NMR (δ, $CDCl_3$, 20°C): 7.25 (t, $^3J_{HH}$ = 7.9 Hz, 1H, py^4), 6.52 (dd, $^3J_{HH}$ = 8.0 Hz, $^4J_{PH}$ = 2.4 Hz, 1H, py^3), 5.89 (d, $^3J_{HH}$ = 7.7 Hz, 1H, py^5), 4.67 (d, $^2J_{PH}$ = 11.0 Hz, 1H, N*H*), 4.19 (s, 2H, NH_2), 1.15 (d, $^3J_{PH}$ = 12.0 Hz, 18H, C(CH_3)$_3$). ^{13}C{^{1}H} NMR (δ, $CDCl_3$, 20°C): 160.25 (d, $^2J_{CP}$ = 21.4 Hz, py^2), 157.29 (d, $^4J_{CP}$ = 1.5 Hz, py^6), 139.39 (d, $^4J_{CP}$ = 2.1 Hz, py^4), 98.36 (d, $^3J_{CP}$ = 18.8 Hz, py^3), 97.96 (py^5), 33.98 (d, $^1J_{CP}$ = 19.2 Hz, *C*(CH$_3$)$_3$), 28.08 (d, $^2J_{CP}$ = 15.2 Hz, C(*C*H$_3$)$_3$). ^{31}P{^{1}H} NMR (δ, $CDCl_3$, 20°C): 58.2. MS (ESI-HRMS, CH_3CN) (m/z): [M+H]$^+$ ($C_{13}H_{25}N_3P$) calcd 254.1786. Found 254.1788.

[PNP-*i*Pr,TAD] (2a). To a solution of **1a** (2.00 g, 8.84 mmol) in toluene (100 mL) NEt_3 (1.9 mL, 13.26 mmol) was added. After cooling to 0°C, a solution of TAD-PCl (5.16 g, 9.72 mmol) in toluene

(30mL) was added and the reaction mixture was stirred overnight at 80°C. The suspension was filtered over a small pad of Celite® and the solvent was removed under reduced pressure. The product was obtained as white powder in sufficient purity for subsequent reactions. If necessary, it can be purified *via* flash chromatography (ethyl acetate/petrol ether/CH_2Cl_2 1:1:1). Yield: 5.75 g (90%). ^{1}H NMR (δ, $CDCl_3$, 20°C): 7.74 – 7.63 (m, 4H, ph), 7.47 – 7.19 (m, 17H, ph, py^4), 6.61 (dd, $^3J_{HH}$ = 8.1 Hz, $^4J_{PH}$ = 2.2 Hz, 1H, py^3), 6.06 (d, $^3J_{HH}$ = 7.7 Hz, 1H, py^5), 5.67 (d, $^2J_{PH}$ = 4.3 Hz, 1H, N*H*^{TAD}), 5.32 (dd, $^3J_{HH}$ = 8.5 Hz, $^4J_{PH}$ = 2.8 Hz, 1H, C*H*^{TAD}), 4.94 (d, $^3J_{HH}$ = 8.5 Hz, 1H, C*H*^{TAD}), 4.43 (d, $^2J_{PH}$ = 11.2 Hz, 1H, N*H*^{iPr}), 1.80 (m, 2H, C*H*$(CH_3)_2^{iPr}$), 1.39 (s, 3H, C*H*$_3^{TAD}$), 1.12 – 1.01 (m, 12H, CH(C*H*$_3)_2^{iPr}$), 0.34 (s, 3H, C*H*$_3^{TAD}$). ^{13}C{^{1}H} NMR (δ, $CDCl_3$, 20°C): 159.96 (d, $^2J_{CP}$ = 20.4 Hz, py^2), 154.19 (d, $^2J_{CP}$ = 16.2 Hz, py^6), 146.42 (Ph^1), 145.58 (Ph^1), 141.62 (Ph^1), 140.95 (Ph^1), 139.12 (py^4), 128.96 (Ph), 128.52 (Ph), 128.49 (Ph), 128.15 (Ph), 127.71 (Ph), 127.67 (Ph), 127.61 (Ph), 127.37 (Ph), 127.28 (Ph), 127.16 (Ph), 112.12 (*C*$(CH_3)_2^{TAD}$), 99.85 (d, $^3J_{CP}$ = 18.8 Hz, py^3), 99.03 (d, $^3J_{CP}$ = 9.3 Hz, py^5), 82.87 (*C*H^{TAD}), 82.68 (*C*Ph_2), 82.46 (*C*H^{TAD}, *C*Ph_2), 27.22 (*C*H_3^{TAD}), 26.37 (d, $^1J_{CP}$ = 10.8 Hz, *C*$H(CH_3)_2^{iPr}$), 26.27 (d, $^1J_{CP}$ = 9.9 Hz, *C*$H(CH_3)_2^{TAD}$), 24.89 (*C*H_3^{TAD}), 18.53 (d, $^2J_{CP}$ = 3.6 Hz, CH(*C*$H_3)_2^{iPr}$), 18.33 (d, $^2J_{CP}$ = 3.8 Hz, CH(*C*$H_3)_2^{iPr}$), 16.99 (d, $^2J_{CP}$ = 8.3 Hz, CH(*C*$H_3)_2^{iPr}$), 16.90 (d, $^2J_{CP}$ = 7.7 Hz, CH(*C*$H_3)_2^{iPr}$). ^{31}P{^{1}H} NMR (δ, $CDCl_3$, 20°C): 134.6 (TAD), 47.9 (*i*Pr). MS (ESI-HRMS, CH_3CN/CH_3OH) (m/z): $[M+H]^+$ ($C_{42}H_{48}N_3O_4P_2$) calcd 720.3115. Found 720.3113.

[PNP-*t*Bu,TAD] (2b). This compound was prepared analogously to **2a** with **1b** (0.86.g, 8.84 mmol), NEt_3 (0.7 mL, 5.08 mmol), and TAD-PCl (1.80 g, 3.38 mmol) as starting materials. Yield: 2.39 g (94%). ^{1}H NMR (δ, $CDCl_3$, 20°C): 7.73 (m, 2H, Ph), 7.64 (m, 2H, Ph), 7.50 – 7.16 (m, 17H, Ph, py^4), 6.63 (dd, $^3J_{HH}$ = 8.0 Hz, $^4J_{PH}$ = 2.2 Hz, 1H, py^3), 6.10 (d, $^3J_{HH}$ = 7.8 Hz, 1H, py^5), 5.55 (d, $^2J_{PH}$ = 2.4 Hz, 1H, N*H*^{TAD}), 5.32 (dd, $^3J_{HH}$ = 8.4 Hz, $^4J_{PH}$ = 2.4 Hz, 1H, C*H*^{TAD}), 4.99 (d, $^3J_{HH}$ = 8.4 Hz, 1H, C*H*^{TAD}), 4.67 (d, $^2J_{PH}$ = 11.2 Hz, 1H, N*H*^{iPr}), 1.22 (s, 3H, C*H*$_3^{TAD}$), 1.17 (d, $^3J_{PH}$ = 4.7 Hz, 9H, C(C*H*$_3)_3^{tBu}$), 1.12 (d, $^3J_{PH}$ = 4.7 Hz, 9H, C(C*H*$_3)_3^{tBu}$), 0.35 (s, 3H, C*H*$_3^{TAD}$). ^{13}C{^{1}H} NMR (δ, $CDCl_3$, 20°C): 160.19 (d, $^2J_{CP}$ = 21.8 Hz, py^2), 153.90 (d, $^2J_{CP}$ = 19.0 Hz, py^6), 145.99 (Ph^1), 145.52 (Ph^1), 141.74 (Ph^1), 140.95 (s, Ph^1), 139.26 (py^4), 128.93 (Ph), 128.54 (Ph), 128.19 (Ph), 127.71 (Ph), 127.47 (Ph), 127.36 (Ph), 127.15 (Ph), 127.06 (Ph), 126.65 (Ph), 112.36 (*C*$(CH_3)_2^{TAD}$), 100.36 (d, $^3J_{CP}$ = 19.2 Hz, py^3), 99.07 (d, $^3J_{CP}$ = 15.2 Hz, py^5), 83.34 (*C*Ph_2), 82.66 (d, $^3J_{CP}$ = 7.6 Hz, *C*H^{TAD}), 82.27 (d, $^3J_{CP}$ = 7.8 Hz, *C*H^{TAD}), 82.12 (*C*Ph_2, 33.96 (d, $^1J_{CP}$ = 19.1 Hz, *C*$(CH_3)_3^{tBu}$), 28.19 (C(*C*$H_3)_3^{tBu}$), 27.95 (C(*C*$H_3)_3^{tBu}$), 27.33 (*C*H_3^{TAD}), 25.39 (*C*H_3^{TAD}). ^{31}P{^{1}H} NMR (δ, $CDCl_3$, 20°C): 132.4 (TAD), 58.6 (*t*Bu). MS (ESI-HRMS, CH_3CN/CH_3OH) (m/z): $[M+H]^+$ ($C_{44}H_{52}N_3O_4P_2$) calcd 748.3428. Found 748.3427.

[Fe(κ^2*P,N*-PNP-*i*Pr,TAD)Cl_2] (3a). A suspension of anhydrous $FeCl_2$ (86 mg, 0.68 mmol) and **2a** (500 mg, 0.69 mmol) was stirred in THF (15 mL) at room temperature for 12 h. The solvent was then removed under vacuum and the remaining solid redissolved in CH_2Cl_2 (15mL). Insoluble materials were removed by filtration. The volume of the solution was reduced to about 1 mL and the product was precipitated by addition of *n*-pentane (40 mL). After filtration the yellow product was washed twice with *n*-pentane (10 mL) and dried under vacuum. Yield: 458 mg (79%). Anal. Calcd. for $C_{42}H_{47}Cl_2N_3O_4P_2Fe$ (846.55): C, 59.59; H, 5.60; N, 4.96%. Found: C, 58.99; H, 5.49; N, 5.10%. ESI-MS (*m/z,* CH_3CN/CH_3OH) positive ion: 868.2 $[M+Na]^+$, 842.3 $[M-Cl+CH_3OH]^+$, 810.2 $[M-Cl]^+$. μ_{eff} = 4.95(1)μ_B.

[Fe(κ²*P,N*-PNP-*i*Pr,TAD)Br₂] (3b). This complex was prepared analogously to **3a** with anhydrous $FeBr_2$ (176 mg, 0.82 mmol) and **2a** (600 mg, 0.83 mmol) as starting materials. Yield: 678 mg (89%). Anal. Calcd. for $C_{42}H_{47}Br_2N_3O_4P_2Fe$ (935.46): C, 53.93; H, 5.06; N, 4.49%. Found: C, 54.09; H, 5.19; N, 4.52%. ESI-MS (*m/z,* CH_3CN/CH_3OH) positive ion: 956.1 $[M+Na]^+$, 886.2 $[M\text{-}Br\text{-}CH_3OH]^+$, 854.2 $[M\text{-}Br]^+$, 806.3 $[M-Br\text{-}HBr+CH_3OH]^+$. μ_{eff} = 4.97(1)μ_B.

[Fe(κ²*P,N*-PNP-*t*Bu,TAD)Cl₂] (4a). This complex was prepared analogously to **3a** with anhydrous $FeCl_2$ (48 mg, 0.38 mmol) and **2b** (300 mg, 0.40 mmol) as starting materials. Yield: 263 mg (79%). Anal. Calcd. for $C_{44}H_{51}Cl_2N_3O_4P_2Fe$ (874.60): C, 60.43; H, 5.88; N, 4.80%. Found: C, 60.22; H, 5.92; N, 4.95%. ESI-MS (*m/z,* CH_3CN/CH_3OH) positive ion: 896.2 $[M+Na]^+$. μ_{eff} = 4.98(1)μ_B.

[Fe(κ²*P,N*-PNP-*t*Bu,TAD)Br₂] (4b). This complex was prepared analogously to **3a** with anhydrous $FeBr_2$ (82 mg, 0.38 mmol) and **2b** (300 mg, 0.40 mmol) as starting materials. Yield: 305 mg (83%). Anal. Calcd. for $C_{44}H_{51}Br_2N_3O_4P_2Fe$ (963.51): C, 54.85; H, 5.34; N, 4.36%. Found: C, 54.92; H, 5.39; N, 4.22%. ESI-MS (*m/z,* CH_3CN/CH_3OH) positive ion: 984.1 $[M+Na]^+$, 882.2 $[M-Br]^+$. μ_{eff} = 5.00(1)μ_B.

Boronation of [Fe(κ²*P,N*-PNP-*i*Pr,TAD)Cl₂] (3a) in CD_2Cl_2. BH_3·THF (26.0 µL, 26.0 µmol, 1.0 M in THF) was transferred to a NMR-tube containing **3a** (20 mg, 23.6 µmol) in CD_2Cl_2 (0.5 mL). A $^{31}P\{^1H\}$ and ^{11}B NMR spectra were immediately measured giving rise to signals at 60.0 and -46.8 ppm, respectively.

***trans*-[Fe(κ³*P,N,P*-PNP-*i*Pr,TAD)(CO)Cl₂] (6a).** A solution of **3a** (200 mg, 0.24 mmol) in THF (5 mL) was purged with CO for 3 min, whereupon the colour changed immediately from yellow to violet. The product was crystallized by slow diffusion of *n*-pentane into a THF solution of **6a**. The solvent was decanted and the remaining solid was dried under vacuum for 30 min. Yield: 152 mg (74%). Anal. Calcd. for $C_{43}H_{47}Cl_2N_3O_5P_2Fe{\cdot}C_4H_8O$ (946.66): C, 59.63; H, 5.86; N, 4.44%. Found: C, 59.52; H, 5.99; N, 4.65%. ^1H NMR (δ, acetone-d_6, 20°C): 8.09 (d, $^2J_{PH}$ = 8.1 Hz, 1H, N*H*^{iPr}), 7.97 (m, 2H, Ph), 7.82 (m, 2H, Ph), 7.74 (d, $^2J_{PH}$ = 3.1 Hz, 1H, N*H*^{TAD}), 7.56-7.47 (m, 4H, Ph), 7.42-7.35 (m, 4H, Ph), 7.29-7.19 (m, 9H, py^4, Ph), 6.56 (d, $^3J_{HH}$ = 7.9 Hz, 1H, py^3), 5.91 (d, $^3J_{HH}$ = 8.0 Hz, 1H, C*H*^{TAD}), 5.87 (d, $^3J_{HH}$ = 7.8 Hz, 1H, py^5), 5.71 (d, $^3J_{HH}$ = 8.0 Hz, 1H, C*H*^{TAD}), 3.14 (m, 1H, C*H*$(CH_3)_2^{iPr}$), 2.98 (m, 1H, C*H*$(CH_3)_2^{iPr}$), 1.55 (dd, $^3J_{HH}$ = 7.0 Hz, $^3J_{PH}$ = 13.7 Hz, 3H, CH(C*H*$_3)_2^{iPr}$), 1.54 (dd, $^3J_{HH}$ = 7.0 Hz, $^3J_{PH}$ = 13.9 Hz, 3H, CH(C*H*$_3)_2^{iPr}$), 1.45 (dd, $^3J_{HH}$ = 7.3 Hz, $^3J_{PH}$ = 16.0 Hz, 3H, CH(C*H*$_3)_2^{iPr}$), 1.36 (dd, $^3J_{HH}$ = 7.3 Hz, $^3J_{PH}$ = 15.9 Hz, 3H, CH(C*H*$_3)_2^{iPr}$), 0.75 (s, 3H, C*H*$_3^{TAD}$), 0.66 (s, 3H, C*H*$_3^{TAD}$). $^{13}C\{^1H\}$ NMR (δ, acetone-d_6, 20°C): 220.32 (dd, $^2J_{CP}$ = 22.3 Hz, $^2J_{CP}$ = 35.1 Hz, *C*O), 162.58 (dd, $^2J_{CP}$ = 8.0 Hz, $^4J_{CP}$ = 12.9 Hz, py^2), 157.81 (dd, $^2J_{CP}$ = 3.3 Hz, $^4J_{CP}$ = 23.5 Hz, py^6), 144.07 (Ph^1), 143.35 (Ph^1), 141.75 (d, $^3J_{CP}$ = 5.5 Hz, Ph^1), 140.29 (d, $^3J_{CP}$ = 8.2 Hz, Ph^1), 139.46 (py^4), 129.02 (Ph), 128.84 (Ph), 128.43 (Ph), 128.36 (Ph), 127.98 (Ph), 127.68 (Ph), 127.61 (Ph), 127.34 (Ph), 127.13 (Ph), 127.05 (Ph), 126.79 (Ph), 126.66 (Ph), 114.62 (*C*$(CH_3)_2$), 99.97 (d, $^3J_{CP}$ = 7.3 Hz, py^3), 98.65 (d, $^3J_{CP}$ = 10.4 Hz, py^5), 88.91 (d, $^2J_{CP}$ = 8.3 Hz, *C*Ph$_2$), 88.56 (d, $^2J_{CP}$ = 19.9 Hz, *C*Ph$_2$), 80.97 (d, $^3J_{CP}$ = 2.5 Hz, *C*H^{TAD}), 79.98 (d, $^3J_{CP}$ = 2.9 Hz, *C*H^{TAD}), 26.44 (*C*H$_3^{TAD}$), 26.01 (*C*H$_3^{TAD}$), 25.86 (d, $^1J_{CP}$ = 22.0 Hz, *C*H$(CH_3)_2^{iPr}$), 24.94 (d, $^1J_{CP}$ = 25.5 Hz, *C*H$(CH_3)_2^{iPr}$), 18.69 (d, $^2J_{CP}$ = 4.3 Hz, CH(*C*H$_3)_2^{iPr}$), 18.61 (d, $^2J_{CP}$ = 3.9 Hz, CH(*C*H$_3)_2^{iPr}$), 17.74 (CH(*C*H$_3)_2^{iPr}$), 17.28 (*C*H$(CH_3)_2^{iPr}$). $^{31}P\{^1H\}$ NMR (δ, $CDCl_3$, 20°C): 154.0 (d, $^2J_{PP}$ =

278.8 Hz, TAD), 125.1 (d, $^{2}J_{PP}$ = 278.9 Hz, *i*Pr). IR (ATR, cm^{-1}): 1976 ($\nu_{C=O}$). IR (CH_2Cl_2, cm^{-1}): 1986 ($\nu_{C=O}$).

***trans*-[Fe(κ^3*P,N,P*-PNP-*i*Pr,TAD)(CO)Br$_2$] (6b).** This compound was prepared analogously to **6a** with **3b** (200 mg, 0.21 mmol) as starting material. Yield: 164 mg (80%). Anal. Calcd. for $C_{43}H_{47}Br_2N_3O_5P_2Fe{\cdot}2C_4H_8O$ (1107.68): C, 55.30; H, 5.73; N, 3.79%. Found: C, 55.52; H, 5.81; N, 3.44%. ^{1}H-NMR (δ, acetone-d_6, 20°C): 8.07 (d, $^{2}J_{PH}$ = 8.1 Hz, 1H, N*H*^{iPr}), 8.02 (m, 2H, ph), 7.89 (m, 2H, ph), 7.76 (dd, $^{2}J_{PH}$ = 6.5 Hz, $^{4}J_{PH}$ = 3.0 Hz, 1H, N*H*^{TAD}), 7.54 (m, 2H, Ph), 7.48 (m, 2H, Ph), 7.39 (m, 4H, Ph), 7.34 (t, $^{3}J_{HH}$ = 7.9 Hz, 1H, py^4), 7.29 – 7.18 (m, 8H, Ph), 6.56 (d, $^{3}J_{HH}$ = 7.9 Hz, 1H, py^3), 5.88 (d, $^{3}J_{HH}$ = 8.0 Hz, 1H, C*H*^{TAD}), 5.82 (d, $^{3}J_{HH}$ = 7.8 Hz, 1H, py^5), 5.72 (d, $^{3}J_{HH}$ = 8.0 Hz, 1H, C*H*^{TAD}), 3.37 (m, 1H, C*H*(CH$_3$)$_2^{iPr}$), 3.19 (m, 1H, C*H*(CH$_3$)$_2^{iPr}$), 1.59 (dd, $^{3}J_{HH}$ = 7.2 Hz, $^{3}J_{PH}$ = 13.6 Hz, 3H, CH(C*H*$_3$)$_2^{iPr}$), 1.53 (dd, $^{3}J_{HH}$ = 7.2 Hz, $^{3}J_{PH}$ = 13.1 Hz, 3H, CH(C*H*$_3$)$_2^{iPr}$), 1.47 (dd, $^{3}J_{HH}$ = 7.4 Hz, $^{3}J_{PH}$ = 16.0 Hz, 3H, CH(C*H*$_3$)$_2^{iPr}$), 1.37 (dd, $^{3}J_{HH}$ = 7.3 Hz, $^{3}J_{PH}$ = 16.2 Hz, 3H, CH(C*H*$_3$)$_2^{iPr}$), 0.72 (s, 3H, C*H*$_3^{TAD}$), 0.65 (s, 3H, C*H*$_3^{TAD}$). ^{13}C{^{1}H} NMR (δ, acetone-d_6, 20°C): 222.53 (dd, $^{2}J_{CP}$ = 22.2 Hz, $^{2}J_{CP}$ = 34.9 Hz, *C*O), 162.58 (dd, $^{2}J_{CP}$ = 12.5 Hz, $^{4}J_{CP}$ = 7.3 Hz, py^2), 157.81 (dd, $^{2}J_{CP}$ = 22.9 Hz, $^{4}J_{CP}$ = 3.3 Hz, py^6), 144.04 (Ph^1), 143.27 (Ph^1), 141.84 (d, $^{3}J_{CP}$ = 5.5 Hz, Ph^1), 140.10 (d, $^{3}J_{CP}$ = 8.2 Hz, Ph^1), 139.34 (py^4), 129.15 (Ph), 129.06 (Ph), 128.70 (Ph), 128.40 (Ph), 127.94 (Ph), 127.72 (Ph), 127.66 (Ph), 127.53 (Ph), 127.16 (Ph), 127.09 (Ph), 126.74 (Ph), 126.65 (Ph), 114.63 (*C*(CH$_3$)$_2$), 100.01 (d, $^{3}J_{CP}$ = 7.5 Hz, py^3), 98.92 (d, $^{3}J_{CP}$ = 10.3 Hz, py^5), 89.38 (d, $^{2}J_{CP}$ = 8.9 Hz, *C*Ph$_2$), 89.27 (d, $^{2}J_{CP}$ = 12.6 Hz, *C*Ph$_2$), 80.36 (d, $^{3}J_{CP}$ = 2.5 Hz, *C*H^{TAD}), 79.74 (d, $^{3}J_{CP}$ = 2.9 Hz, *C*H^{TAD}), 28.26 (d, $^{1}J_{CP}$ = 21.7 Hz, *C*H(CH$_3$)$_2^{iPr}$), 26.89 (d, $^{1}J_{CP}$ = 26.8 Hz, *C*H(CH$_3$)$_2^{iPr}$), 26.42 (*C*H$_3^{TAD}$), 26.07 (*C*H$_3^{TAD}$), 18.84 (d, $^{2}J_{CP}$ = 3.9 Hz, CH(*C*H$_3$)$_2^{iPr}$), 18.50 (d, $^{2}J_{CP}$ = 4.3 Hz, CH(*C*H$_3$)$_2^{iPr}$), 18.06 (CH(*C*H$_3$)$_2^{iPr}$), 17.42 (s, *C*H(CH$_3$)$_2^{iPr}$). ^{31}P{^{1}H} NMR (δ, $CDCl_3$, 20°C): 161.61 (d, $^{2}J_{PP}$ = 261.4 Hz, TAD), 125.20 (d, $^{2}J_{PP}$ = 261.4 Hz, iPr). IR (ATR, cm^{-1}): 1967 ($\nu_{C=O}$). IR (CH_2Cl_2, cm^{-1}): 1980 ($\nu_{C=O}$).

***trans*-[Fe(κ^3*P,N,P*-PNP-*i*Pr,TAD)(CO)$_2$Cl]SbF$_6$ (7a).** CO was bubbled through a solution of **3a** (200 mg, 0.24 mmol) and $AgSbF_6$ (82 mg, 0.24 mmol) in THF (15 mL) for 5 min. The solvent was removed under vacuum and, the pink precipitate was dissolved in 15 mL of CH_2Cl_2. Insoluble materials were removed by filtration and the volume of the solution was then reduced to about one mL. The product was precipitated upon addition of n-hexane (40 mL) and dried under vacuum for 2 h. Yield: 210 mg (81%). Anal. Calcd. for $C_{44}H_{47}ClF_6N_3O_6P_2FeSb$ (1102.87): C, 47.92; H, 4.30; N, 3.81%. Found: C, 47.82; H, 4.22; N, 3.89%. ^{1}H NMR (δ, CD_2Cl_2, 20°C): 7.58 – 7.56 (m, 2H, Ph), 7.50 – 7.48 (m, 2H, Ph), 7.38 – 7.25 (m, 16H, Ph), 7.18 (bs, 1H, py^4), 6.37 (m, 2H, N*H*^{TAD}, py^3), 5.67 (d, $^{2}J_{PH}$ = 8.1 Hz, 1H, N*H*^{iPr}), 5.60 (d, $^{3}J_{HH}$ = 7.2 Hz, 1H, py^5), 5.52 (d, $^{3}J_{HH}$ = 7.8 Hz, 1H, C*H*^{TAD}), 5.48 (d, $^{3}J_{HH}$ = 7.8 Hz, 1H, C*H*^{TAD}), 3.05 – 2.83 (m, 2H, C*H*(CH$_3$)$_2^{iPr}$), 1.47 – 1.30 (m, 12H, CH(C*H*$_3$)$_2^{iPr}$), 0.78 (s, 3H, C*H*$_3^{TAD}$), 0.37 (s, 3H, C*H*$_3^{TAD}$). ^{13}C{^{1}H} NMR (δ, CD_2Cl_2, 20°C): 207.44 (dd, $^{2}J_{CP}$ = 23.8 Hz, $^{2}J_{CP}$ = 36.6 Hz, *C*O), 207.08 (dd, $^{2}J_{CP}$ = 24.4 Hz, $^{2}J_{CP}$ = 38.0 Hz, *C*O), 161.78 (m, py^2), 156.10 (dd, $^{2}J_{CP}$ = 18.2 Hz, $^{4}J_{CP}$ = 2.7 Hz, py^6), 142.73 (py^4), 141.95 (Ph^1), 141.72 (d, $^{3}J_{CP}$ = 2.3 Hz, Ph^1), 139.19 (d, $^{3}J_{CP}$ = 4.5 Hz, Ph^1), 138.90 (d, $^{3}J_{CP}$ = 8.7 Hz, Ph^1), 129.52 (Ph), 129.28 (Ph),129.07 (Ph), 129.05 (Ph), 128.57 (Ph), 128.54 (Ph), 128.42 (Ph), 128.31 (Ph), 128.20 (Ph), 127.71 (Ph), 127.67 (Ph), 126.94 (Ph), 115.79 (s, *C*(CH$_3$)$_2$), 102.54 (d, $^{3}J_{CP}$ = 11.2 Hz, $^{5}J_{CP}$ = 6.8 Hz, py^3), 100.24 (d, $^{3}J_{CP}$ = 9.0 Hz, $^{5}J_{CP}$ = 3.3 Hz, py^5), 93.68 (d, $^{2}J_{CP}$ = 13.0 Hz, *C*Ph$_2$), 93.12 (d, $^{2}J_{CP}$ = 19.5 Hz, *C*Ph$_2$), 79.47 (d, $^{3}J_{CP}$ = 3.6 Hz,

*C*H^{TAD}), 78.22 (d, $^{3}J_{CP}$ = 3.2 Hz, *C*H^{TAD}), 32.16 (dd, $^{1}J_{CP}$ = 23.4 Hz, $^{3}J_{CP}$ = 1.9 Hz, *C*H(CH$_3$)$_2^{iPr}$), 31.84 (d, $^{1}J_{CP}$ = 21.8 Hz, *C*H(CH$_3$)$_2^{iPr}$), 26.82 (*C*H$_3^{TAD}$), 25.80 (*C*H$_3^{TAD}$), 17.68 – 17.48 (m, $^{2}J_{CP}$ = 1.1 Hz, CH(*C*H$_3$)$_2^{iPr}$). ^{31}P{^{1}H} NMR (δ, CD_2Cl_2, 20°C): 144.66 (d, $^{2}J_{PP}$ = 175.9 Hz, TAD), 111.87 (d, $^{2}J_{PP}$ = 175.9 Hz, iPr). IR (ATR, cm^{-1}): 2026 ($\nu_{C=O}$).

***trans*-[Fe(κ^3*P,N,P*-PNP-*i*Pr,TAD)(CO)$_2$Br]SbF$_6$ (7b).** This complex was prepared analogously to **7a** with **3b** (200 mg, 0.21 mmol) as starting material. Yield: 180 mg (73%). Anal. Calcd. for Anal. Calcd. for $C_{44}H_{47}BrF_6N_3O_6P_2FeSb$ (1147.32): C, 46.06; H, 4.13; N, 3.66%. Found: C, 46.00; H, 4.20; N, 3.70%. ^{1}H NMR (δ, CD_2Cl_2, 20°C): 7.57 - 7.55 (m, 2H, Ph), 7.51 – 7.48 (m, 2H, Ph), 7.41 – 7.25 (m, 16H, Ph), 7.21 (d, $^{3}J_{HH}$ = 8.1 Hz, 1H, py^4), 6.44 (d, $^{2}J_{PH}$ = 2.2 Hz, 1H, N*H*^{TAD}), 6.40 (d, $^{3}J_{HH}$ = 8.1 Hz, 1H, py^3), 5.66 (d, $^{2}J_{PH}$ = 8.5 Hz, 1H, N*H*^{iPr}), 5.62 (d, $^{3}J_{HH}$ = 8.0 Hz, 1H, py^5), 5.50 (d, $^{3}J_{HH}$ = 7.8 Hz, 1H, C*H*^{TAD}), 5.46 (d, $^{3}J_{HH}$ = 7.8 Hz, 1H, C*H*^{TAD}), 3.00 – 2.84 (m, 2H, C*H*(CH$_3$)$_2^{iPr}$), 1.47 (dd, $^{3}J_{HH}$ = 7.1 Hz, $^{3}J_{PH}$ = 3.0 Hz, 3H, CH(C*H*$_3$)$_2^{iPr}$), 1.43 (dd, $^{3}J_{HH}$ = 7.1 Hz, $^{3}J_{PH}$ = 4.2 Hz, 3H, CH(C*H*$_3$)$_2^{iPr}$), 1.39 (dd, $^{3}J_{HH}$ = 7.2 Hz, $^{3}J_{PH}$ = 15.4 Hz, 3H, CH(C*H*$_3$)$_2^{iPr}$), 1.35 (dd, $^{3}J_{HH}$ = 7.1 Hz, $^{3}J_{PH}$ = 16.3 Hz, 3H, CH(C*H*$_3$)$_2^{iPr}$), 0.80 (s, 3H, C*H*$_3^{TAD}$), 0.37 (s, 3H, C*H*$_3^{TAD}$). ^{13}C{^{1}H} NMR (δ, CD_2Cl_2, 20°C): 207.76 (dd, $^{2}J_{CP}$ = 21.2 Hz, $^{2}J_{CP}$ = 37.9 Hz, *C*O), 207.38 (dd, $^{2}J_{CP}$ = 23.8 Hz, $^{2}J_{CP}$ = 42.3 Hz, *C*O), 161.75 (dd, $^{2}J_{CP}$ = 8.1 Hz, $^{4}J_{CP}$ = 6.2 Hz, py^2), 156.14 (dd, $^{2}J_{CP}$ = 18.5 Hz, $^{4}J_{CP}$ = 2.9 Hz, py^6), 142.77 (Ph^1), 141.90 (py^4), 141.87 (Ph^1), 139.23 (d, $^{3}J_{CP}$ = 4.3 Hz, Ph^1), 138.91 (d, $^{3}J_{CP}$ = 8.8 Hz, Ph^1), 129.51 (Ph), 129.28 (Ph), 129.06 (Ph), 129.00 (Ph), 128.61 (Ph), 128.54 (Ph), 128.43 (Ph), 128.35 (Ph), 128.21 (Ph), 127.69 (Ph), 126.91 (Ph), 115.77 (*C*(CH$_3$)$_2$), 102.50 (d, $^{3}J_{CP}$ = 6.3 Hz, py^3), 100.18 (d, $^{3}J_{CP}$ = 9.2 Hz, py^5), 94.01 (d, $^{2}J_{CP}$ = 13.8 Hz, *C*Ph$_2$), 93.02 (d, $^{2}J_{CP}$ = 19.6 Hz, *C*Ph$_2$), 79.52 (d, $^{3}J_{CP}$ = 3.7 Hz, *C*H^{TAD}), 78.25 (d, $^{3}J_{CP}$ = 3.3 Hz, *C*H^{TAD}), 32.44 (dd, $^{1}J_{CP}$ = 23.7 Hz, $^{3}J_{CP}$ = 3.2Hz, *C*H(CH$_3$)$_2^{iPr}$), 32.12 (dd, $^{1}J_{CP}$ = 22.4 Hz, $^{3}J_{CP}$ = 3.2Hz, *C*H(CH$_3$)$_2^{iPr}$), 26.85 (*C*H$_3^{TAD}$), 25.77 (*C*H$_3^{TAD}$), 18.01 (d, $^{2}J_{CP}$ = 1.1 Hz, CH(*C*H$_3$)$_2^{iPr}$), 17.92 (bs, CH(*C*H$_3$)$_2^{iPr}$), 17.86 (CH(*C*H$_3$)$_2^{iPr}$), 17.84 (*C*H(CH$_3$)$_2^{iPr}$). ^{31}P{^{1}H} NMR (δ, CD_2Cl_2, 20°C): 144.66 (d, $^{2}J_{PP}$ = 169.8 Hz, TAD), 113.36 (d, $^{2}J_{PP}$ = 169.9 Hz, *i*Pr). IR (ATR, cm^{-1}): 2021 ($\nu_{C=O}$).

X-ray Structure Determination. X-ray diffraction data of **3b**·THF, **4a**·THF and **6b**·2THF were collected at *T* = 100 K in a dry stream of nitrogen on Bruker Kappa APEX II diffractometer systems using graphite-monochromatized Mo-*K*α radiation (λ = 0.71073 Å) and fine sliced *φ*- and *ω*-scans. Data were reduced to intensity values with SAINT and an absorption correction was applied with the multi-scan approach implemented in SADABS.[16] The structures were solved by charge flipping using SUPERFLIP[17] and refined against *F* with JANA2006.[18] Non-hydrogen atoms were refined anisotropically. The H atoms connected to C atoms were placed in calculated positions and thereafter refined as riding on the parent atoms. H atoms connected to N located in difference Fourier maps. In **3b**·THF and **4a**·THF they were refined as riding on the parent N atom whereas in **6b**·2THF the positions were refined with the N–H distance restrained to 0.870(1) Å. Molecular graphics were generated with the program MERCURY.[19] Crystal data and experimental details are given in Table S1.

Computational Details Calculations were performed using the GAUSSIAN 09 software package,[20] and the B3LYP functional[21] without symmetry constraints. This functional was shown to perform well in mechanistic studies of spin forbidden reactions in closely related Fe system.[9] The optimized geometries were obtained with the Stuttgart/Dresden ECP (SDD) basis set[22] to describe the electrons of the iron atom. For all other atoms a standard 6-31G** basis set was employed.[23]

Transition state optimizations were performed with the Synchronous Transit-Guided Quasi-Newton Method (STQN) developed by Schlegel *et al*,[24] following a thorough search of the Potential Energy Surfaces (PES). Frequency calculations were performed to confirm the nature of the stationary points, yielding one imaginary frequency for the transition states and none for the minima. Each transition state was further confirmed by following its vibrational mode downhill on both sides, and obtaining the minima presented on the energy profiles.

The Minimum Energy Crossing Points (MECP) between PES of two different spin states were determined using a code developed by Harvey *et al.*[25] This code consists of a set of shell scripts and Fortran programs that use the Gaussian results of energies and gradients of both spin states to produce an effective gradient pointing towards the MECP. The energy values presented in the energy profiles correspond to electronic energy, since MECP are not stationary points and, hence, a standard frequency analysis is not applicable.

Mössbauer parameters (quadrupole splittings and isomer shifts) were evaluated by performing single-point calculations at the B3LYP[21] level of theory with the ORCA software (Version 2.9.0),[26] on the optimized geometries. The value for quadrupole splittings is directly given by the program, while the isomer shift was evaluated from the electron density at the Fe nucleus using the approach of Neese.[27] Fe was described by the triply polarized core properties basis set CP(PPP)[28] and the other atoms by the SV(P) basis set[29] with the inner s-functions uncontracted; the auxiliary basis set SV/J[30] was also used for these calculations. For the Fe atom, an enhanced integration grid was used, and the overall integration accuracy was increased to 7.

Acknowledgements. Financial support by the Austrian Science Fund (FWF) is gratefully acknowledged (Projects No. P24583-N28 and P24202-N17). The X-ray center of the Vienna University of Technology is acknowledged for financial support and for providing access to the single-crystal diffractometer. MDC, LPF and LFV acknowledge Fundação para a Ciência e Tecnologia, Projecto Estratégico FCT (PEst-OE/QUI/UI0612/2013, PEst-OE/FIS/UI0261/2011 and PEst-OE/QUI/UI0100/2013) for financial support. The support and sponsorship of COST action CM1205 “Catalytic Routines for Small Molecule Activation (CARISMA)” is also acknowledged.

†Electronic supplementary information (ESI) available. Complete crystallographic data and technical details in CIF format for **3b**·THF**, 4a**·THF, and **6b**·2THF (CCDC entries 1032898-1032900). ^{1}H, ^{13}C{^{1}H}, and ^{31}P{^{1}H} NMR spectra of all complexes. Atomic coordinates for all DFT optimized structures. For ESI and crystallographic data in CIF or other electronic format see DOI: xxxxxxx

Figures

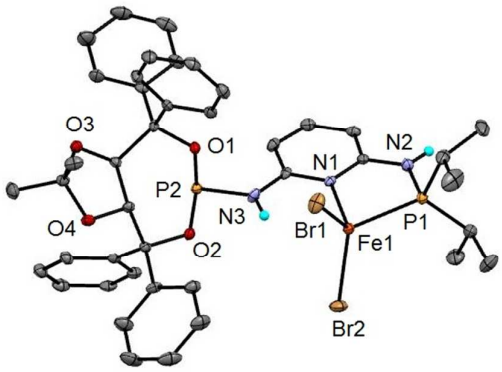

Figure 1. Structural view of [Fe(κ^2*P,N*-PNP-*i*Pr,TAD)Br_2]·THF (**3b**·THF) showing 50% thermal ellipsoids (most H atoms and solvent molecules omitted for clarity). Only one of the two crystallographically independent complexes is shown. Selected bond lengths (Å) and bond angles (°): Fe1-Br1 2.3571(5), Fe1-Br2 2.3785(5), Fe1-P1 2.3776(8), Fe1-N1 2.125(2), N1-Fe1-P1 81.37(6), Br1-Fe1-Br2 117.78(2).

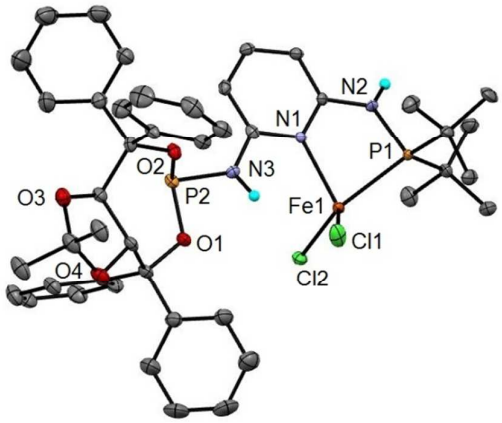

Figure 2. Structural view of [Fe(κ^2*P,N*-PNP-*t*Bu,TAD)Cl_2]·THF (**4a**·THF) showing 50% thermal ellipsoids (most H atoms and solvent molecules omitted for clarity). Selected bond lengths (Å) and bond angles (°): Fe1-Cl1 2.2389(8), Fe1-Cl2 2.2453(8), Fe1-P1 2.4150(8), Fe1-N1 2.120(2), N1-Fe1-P1 80.43(5), Cl1-Fe1-Cl2 115.70(3).

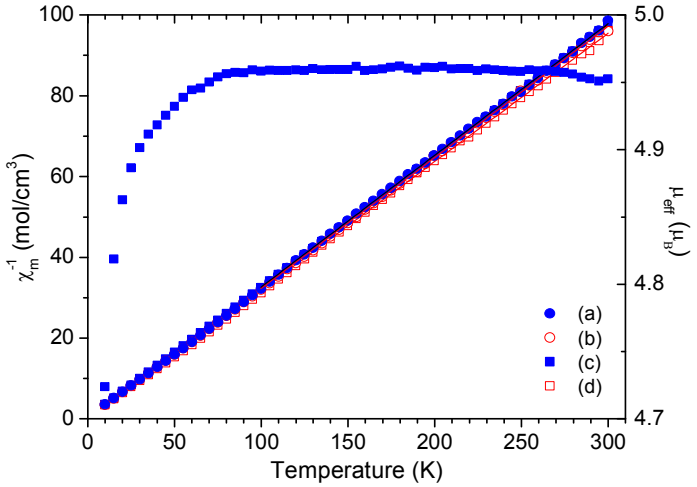

Figure 3. Temperature dependence of the inverse molar susceptibility of (a) [Fe(κ^2*P,N*-PNP-*i*Pr,TAD)Cl$_2$] (**3a**), (b) [Fe(κ^2*P,N*-PNP-*i*Pr,TAD)Br$_2$] (**3b**), (c) [Fe(κ^2*P,N*-PNP-*t*Bu,TAD)Cl$_2$] (**4a**), and (d) [Fe(κ^2*P,N*-PNP-*t*Bu,TAD)Br$_2$] (**4b**), and of the effective magnetic moment of **4a**. The straight lines correspond to Curie law fittings to the experimental data.

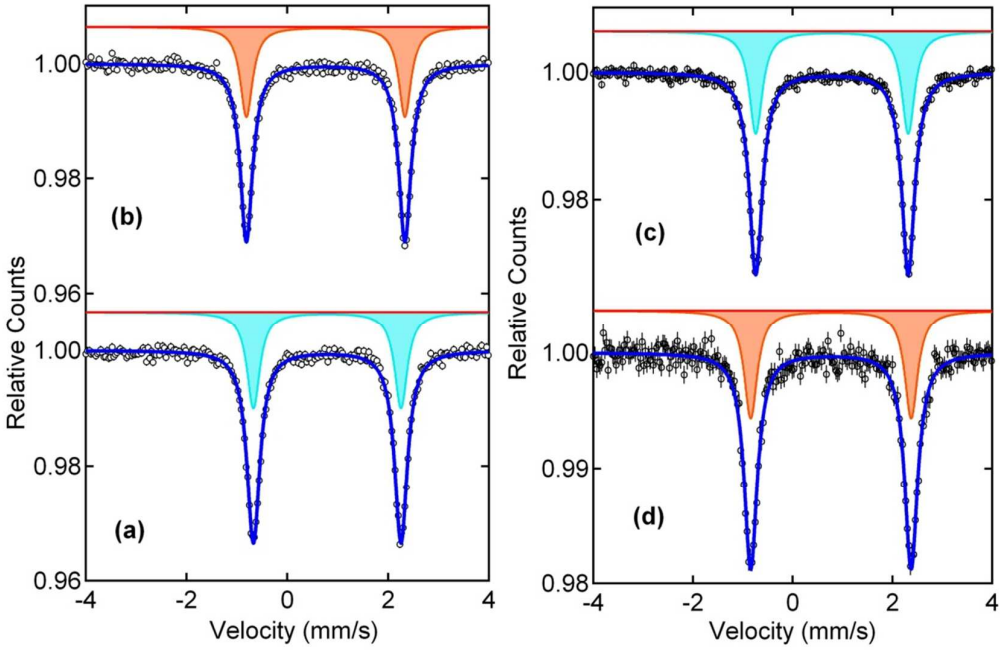

Figure 4. ^{57}Fe Mössbauer spectra of (a) [Fe(κ^2*P,N*-PNP-*i*Pr,TAD)Cl$_2$] (**3a**), (b) [Fe(κ^2*P,N*-PNP-*i*Pr,TAD)Br$_2$] (**3b**), (c) [Fe(κ^2*P,N*-PNP-*t*Bu,TAD)Cl$_2$] (**4a**), and (d) [Fe(κ^2*P,N*-PNP-*t*Bu,TAD)Br$_2$] (**4b**) collected at 78 K.

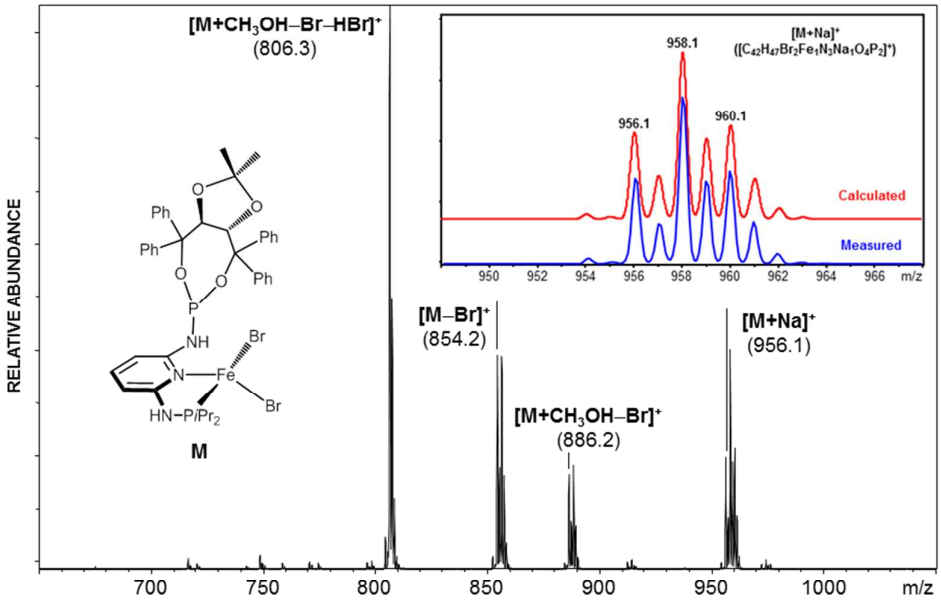

Figure 5. Positive-ion ESI full scan mass spectrum of [Fe(PNP-*i*Pr,TAD)Br_2] (**3b**) in CH_3OH/CH_3CN (9/1). Inset shows the calculated and measured isotopic pattern of the sodiated complex [Fe(PNP-*i*Pr,TAD)Br_2] ($[M+Na]^+$). Only signals containing the Fe isotopes of highest abundance (^{56}Fe) are annotated.

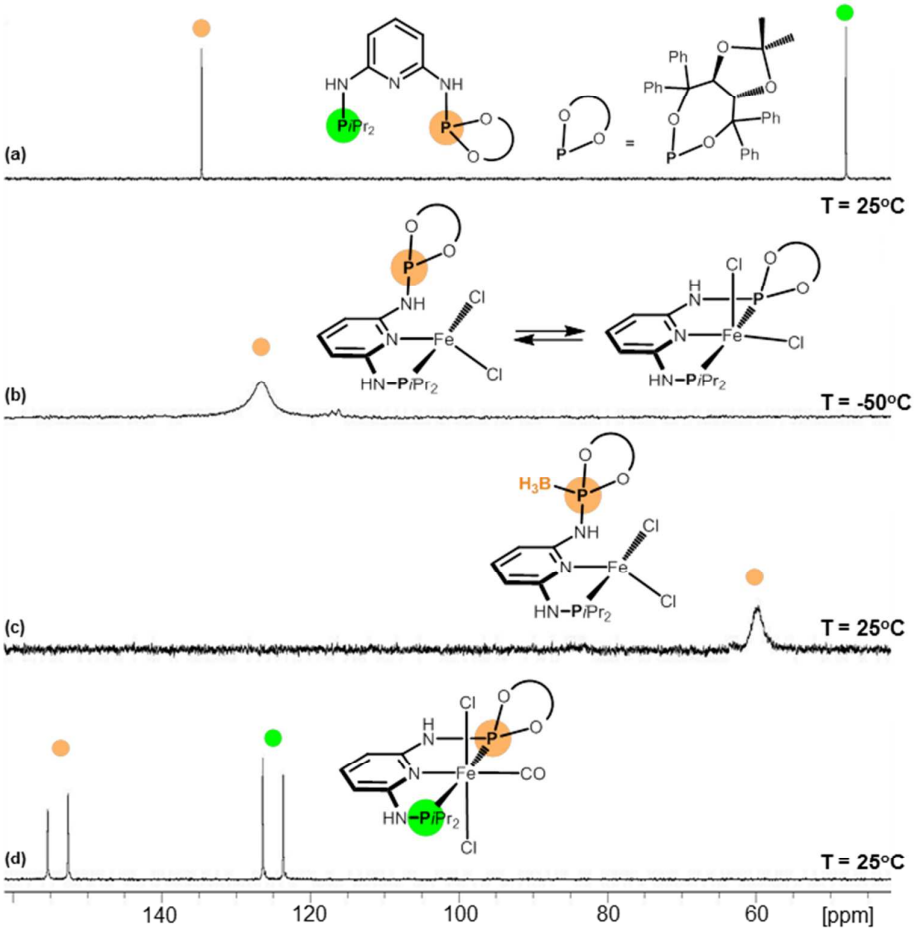

Figure 6 $^{31}P\{^{1}H\}$ NMR spectra of (a) PNP-*i*Pr,TAD (**2a**), (b) [Fe(κ^2*P,N*-PNP-*i*Pr,TAD)Cl_2] (**3a**), (c) [Fe(κ^2*P,N*-PNP^{BH3}-*i*Pr,TAD)Cl_2] (**5**), and (d) *trans*-[Fe(κ^3*P,N,P*-PNP-*i*Pr,TAD)(CO)Cl_2] (**6a**) in CD_2Cl_2 (spectra of **3a** and **5** are referenced internally to PPh_3 set to -5.6 ppm).

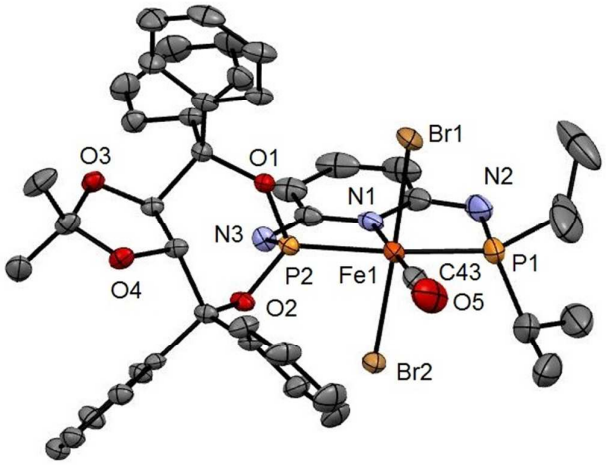

Figure 7. Structural view of *trans*-[Fe(κ^3*P,N,P*-PNP-*i*Pr,TAD)(CO)Br_2]·2THF (**6b**·2THF) showing 50% thermal ellipsoids (H atoms and solvent molecules omitted for clarity). Selected bond lengths (Å) and bond angles (°): Fe1-Br1 2.4508(9), Fe1-Br2 2.4482(8), Fe1-C43 1.766(4), Fe1-P1 2.258(1), Fe1-P2 2.201(1), Fe1-N1 1.996(3), P1-Fe1-P2 163.91(4), N1-Fe1-C43 179.3(1), Br1-Fe1-Br2 177.33(2).

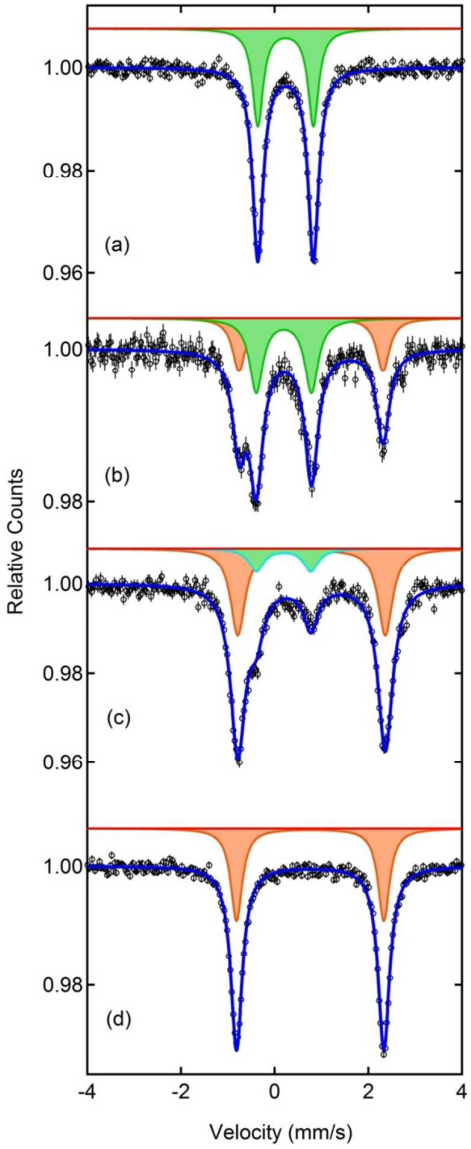

Figure 8. ^{57}Fe Mössbauer spectra collected at 78 K of (a) *trans*-[Fe(κ^3*P,N*-PNP-*i*Pr,TAD)(CO)Br$_2$] (**6b**), (b) and (c) *trans*-[Fe(κ^3*P,N*-PNP-*i*Pr,TAD)(CO)Br$_2$] (**6b**) after heating for 1h and 2h at 100°C under vacuum, respectively, and (d) [Fe(κ^2*P,N*-PNP-*i*Pr,TAD)Br$_2$] (**3b**).

Table 1. Estimated hyperfine parameters from the ^{57}Fe Mössbauer spectra of **3a**, **3b**, **4a**, **4b** and **6b** collected at 78 K and related Fe(II) complexes. IS: isomer shift; QS: quadrupole splitting.

complex	T (K)	IS (mm/s)	QS (mm/s)	Fe(II)	geometry
[Fe(κ^2*P,N*-PNP-*i*Pr,TAD)Cl_2] (**3a**)	78	0.78(1)	2.93(1)	HS	tetrahedral
[Fe(κ^2*P,N*-PNP-*i*Pr,TAD)Br_2] (**3b**)	78	0.76(1)	3.14(1)	HS	tetrahedral
[Fe(κ^2*P,N*-PNP-*t*Bu,TAD)Cl_2] (**4a**)	78	0.79(1)	3.06(1)	HS	tetrahedral
[Fe(κ^2*P,N*-PNP-*t*Bu,TAD)Br_2] (**4b**)	78	0.77(1)	3.22(1)	HS	tetrahedral
trans-[Fe(κ^3*P,N,P*-PNP-*i*Pr,TAD)(CO)Br_2] (**6b**)	78	0.23(1)	1.19(1)	LS	octahedral
[Fe(κ^3*P,N,P*-PNP-*i*Pr)Cl_2][a]	298	0.80(1)	2.56(1)	HS	square pyramidal
[Fe(κ^2*P,N*-PN-*i*Pr)Cl_2][b]	298	0.680(2)	2.871(4)	HS	tetrahedral
[Fe((κ^3*N,N,N*-^{iPr}PDI)Cl_2][c]	80	0.89	2.40	HS	square pyramidal
[Fe(κ^3*N,N,N*-HN{CH_2CH_2($PiPr_2$)})Cl_2][d]	80	0.86	2.89	HS	square pyramidal
[Fe(κ^3*N,N,N*-HN{CH_2CH_2(PCy_2)})Cl_2][d]	80	0.86	2.98	HS	square pyramidal
[Fe(κ^3*N,N,N*-HN{CH_2CH_2($PtBu_2$)})Cl_2][d]	80	0.99	2.69	HS	square pyramidal
trans-[Fe(κ^3*P,N,P*-PNP-*i*Pr)(CO)Cl_2][a]	298	0.15(1)	1.56(1)	LS	octahedral
cis-[Fe(κ^3*P,N,P*-PNP-*i*Pr)(CO)Cl_2][a]	298	0.13(1)	1.09(1)	LS	octahedral
trans-[Fe(κ^2*P,N*-PN^{Me}-Ph)$_2Cl_2$][e]	298	0.85(1)	3.04(1)	HS	octahedral
trans-[Fe(κ^2*P,N*-PN^{Me}-Ph)$_2Br_2$][e]	298	0.88(1)	3.14(1)	HS	octahedral

[a]Ref. 5c, PNP-*i*Pr = N,N'-bis(di-*iso*-propylphosphino)-2,6-diaminopyridine. [b]Ref. 13, PN-*i*Pr = *N*-di-*iso*-propylphosphino-2-aminopyridine. [c]Ref. 31, ^{iPr}PDI = 2,6-(2,6-$iPr_2C_6H_3N{=}CCH_3)_2C_5H_3N$. [d]Ref 32.
[e]Ref. 33, PN^{Me}-Ph = *N*-diphenylphosphino-*N*-methyl-2-aminopyridine.

References

1 For reviews on pincer complexes, see: (a) M. Albrecht and G. van Koten, *Angew. Chem., Int. Ed.* 2001, **40**, 3750. (b) M. E. van der Boom and D. Milstein, *Chem. Rev.* 2003, **103**, 1759. (c) J. T. Singleton, *Tetrahedron* 2003, **59**, 1837. (d) P. Bhattacharya and H. Guan, *Comment Inorg. Chem.* 2011, **32**, 88. (e) S. Schneider, J. Meiners and B. Askevold, *Eur. J. Inorg. Chem.* 2012, 412. (f) D. Morales-Morales and C. M. Jensen, Eds. The Chemistry of Pincer Compounds; Elsevier: Amsterdam, 2007. (g) D. Benito-Garagorri and K. Kirchner, *Acc. Chem. Res.* 2008, **41**, 201.

2 (a) W. V. Dahlhoff and S. M. Nelson, *J. Chem. Soc. (A)*, 1971, 2184. (b) P. Giannoccaro, G. Vasapollo, C. F. Nobile and A. Sacco, *Inorg. Chim. Acta.* 1982, **61**, 69. (c) G. Müller, M. Klinga, M. Leskelä and B. Z. Rieger, *Anorg. Allg. Chem.* 2002, **628**, 2839.

3 (a) J. Zhang, M. Gandelman, D. Herrman, G. Leitus, L. J. W. Shimon, Y. Ben-David and D. Milstein, *Inorg. Chim. Acta* 2006, **359**, 1955. (b) R. J. Trovitch, E. Lobkovsky and P. J. Chirik, *Inorg. Chem*. 2006, **45**, 7252.

4 E. M. Pelczar, T. J. Emge, K. Krogh-Jespersen and A. S. Goldman, *Organometallics* 2008, **27**, 5759.

5 (a) D. Benito-Garagorri, J. Wiedermann, M. Pollak, K. Mereiter and K. Kirchner, *Organometallics* 2007, **26**, 217. (b) D. Benito-Garagorri, M. Puchberger, K. Mereiter and K. Kirchner, *Angew. Chem., Int. Ed.*, 2008, **47**, 9142. (c) D. Benito-Garagorri, L. G. Alves, M. Puchberger, K. Mereiter, L. F. Veiros, M. J. Calhorda, M. D. Carvalho, L. P. Ferreira, M. Godinho and K. Kirchner, *Organometallics* 2009, **28**, 6902.

6 (a) B. Bichler, M. Glatz, B. Stöger, K. Mereiter, L. F. Veiros and K. Kirchner, *Dalton Trans* 2014*,* **43**, 14517. (b) M. Glatz, B. Bichler, M. Mastalir, B. Stöger, K. Mereiter, M. Weil, E. Pittenauer, G. Allmaier, L. F. Veiros and K. Kirchner, *Dalton Trans* 2015*,* **44**, 281.

7 C. Holzhacker, M. J. Calhorda, A. Gil, M. D. Carvalho, L. P. Ferreira, K. Mereiter, B. Stöger, E. Pittenauer, G. Allmaier and K. Kirchner, *Polyhedron* 2014, **81**, 45.

8 W.-S. DeRieux, A. Wong and Y. Schrodi, *J. Organomet. Chem.* 2014, **772-773**, 60.

9 D. Benito-Garagorri, L. G. Alves, L. F. Veiros, C. M. Standfest-Hauser, S. Tanaka, K. Mereiter and K. Kirchner, *Organometallics* 2010, **29**, 4932.

10 N. Gorgas, B. Stöger, E. Pittenauer, G. Allmaier, L. F. Veiros and K. Kirchner, *Organometallics* 2014, **33**, 6905.

11 R. G. Parr and W. Yang, *Density Functional Theory of Atoms and Molecules*, Oxford University Press, New York, 1989.

12 C. Holzhacker, C. M. Standfest-Hauser, M. Puchberger, K. Mereiter, L. F. Veiros, M. J. Calhorda, M. D. Carvalho, L. P. Ferreira, M. Godinho, F. Hartl and K. A. Kirchner, *Organometallics* 2011, **30**, 6587.

13 D. Benito-Garagorri, I. Lagoja, L. F. Veiros and K. A. Kirchner, *Dalton Trans.* 2011, **40**, 4778.

14 D. D. Perrin and W. L. F. Armarego, *Purification of Laboratory Chemicals*, 3rd ed.; Pergamon: New York, 1988.

15 R. Kranich, K. Eis, O. Geis, S. Mühle, J. W. Bats and H.-G. Schmalz, *Chem. Eur. J*. 2000, **6**, 15, 2874.

16 Bruker computer programs: APEX2, SAINT and SADABS (Bruker AXS Inc., Madison, WI, 2012).

17 L. Palatinus and G. Chapuis *J. Appl. Cryst.* 2007, **40**, 786.

18 Petříček, V.; Dušek, M.; Palatinus, L. JANA2006, the crystallographic computing system. (Institute of Physics, Praha, Czeck Republic, 2006)

19 C. F. Macrae, P. R. Edgington, P. McCabe, E. Pidcock, G. P. Shields, R. Taylor, M. Towler and J. van de Streek, *J. Appl. Cryst.* 2006, **39** 453.

20 Gaussian 09, Revision A.02, M. J. Frisch, G. W. Trucks, H. B. Schlegel, G. E. Scuseria, M. A. Robb, J. R. Cheeseman, G. Scalmani, V. Barone, B. Mennucci, G. A. Petersson, H. Nakatsuji, M. Caricato, X. Li, H. P. Hratchian, A. F. Izmaylov, J. Bloino, G. Zheng, J. L. Sonnenberg, M. Hada, M. Ehara, K. Toyota, R. Fukuda, J. Hasegawa, M. Ishida, T. Nakajima, Y. Honda, O. Kitao, H. Nakai, T. Vreven, J. A. Montgomery, Jr., J. E. Peralta, F. Ogliaro, M. Bearpark, J. J. Heyd, E. Brothers, K. N. Kudin, V. N. Staroverov, R. Kobayashi, J. Normand, K. Raghavachari, A. Rendell, J. C. Burant, S. S. Iyengar, J. Tomasi, M. Cossi, N. Rega, J. M. Millam, M. Klene, J. E. Knox, J. B. Cross, V. Bakken, C. Adamo, J. Jaramillo, R. Gomperts, R. E. Stratmann, O. Yazyev, A. J. Austin, R. Cammi, C. Pomelli, J. W. Ochterski, R. L. Martin, K. Morokuma, V. G. Zakrzewski, G. A. Voth, P. Salvador, J. J. Dannenberg, S. Dapprich, A. D. Daniels, Ö. Farkas, J. B. Foresman, J. V. Ortiz, J. Cioslowski, and D. J. Fox, Gaussian, Inc., Wallingford CT, 2009.

21 (a) A. D. Becke, *J. Chem. Phys.* 1993, **98**, 5648. (b) B. Miehlich, A. Savin, H. Stoll and H. Preuss, *Chem. Phys. Lett* 1989, **157**, 200. (c) C. Lee, W. Yang and G. Parr, *Phys. Rev. B* 1988, **37**, 785.

22 (a) U. Haeusermann, M. Dolg, H. Stoll and H. Preuss, *Mol. Phys.* 1993, **78**, 1211; (b) W. Kuechle, M. Dolg, H. Stoll and H. Preuss, *J. Chem. Phys.* 1994, **100**, 7535; (c) T. Leininger, A. Nicklass, H. Stoll, M. Dolg and P. Schwerdtfeger, *J. Chem. Phys.* 1996, **105**, 1052.

23 (a) A. D. McLean and G. S. Chandler, *J. Chem. Phys.* 1980, **72**, 5639. (b) R. Krishnan, J. S. Binkley, R. Seeger and J. A. Pople, *J. Chem. Phys.* 1980, **72**, 650. (c) P. J. Hay, *J. Chem. Phys.* 1977, **66**, 4377. (d) K. Raghavachari and G. W. Trucks, *J. Chem. Phys.* 1989, **91**, 1062. (e) R. C. Binning and L. A. Curtiss, *J. Comput. Chem.* 1995, *10*3, 6104. (f) M. P. McGrath and L. Radom, *J. Chem. Phys.* 1991, **94**, 511.

24 (a) C. Peng, P. Y. Ayala, H. B. Schlegel and M. J. Frisch, *J. Comp. Chem.*, 1996, **17**, 49. (b) C. Peng and H. B. Schlegel, *Israel J. Chem.* 1994, **33**, 449.

25 J. N. Harvey, M. Aschi, H. Schwarz and W. Koch, *Theor. Chem. Acc.* 1998, **99**, 95.

26 Neese, F. ORCA – an ab initio, Density Functional and Semi-empirical Program Package, Version 2.9.0, January 2012, Max-Planck-Institut für Bioanorganische Chemie, Mülheim/Ruhr, 2012.

27 (a) F. Neese, *Inorg. Chim. Acta* 2002, **337**, 181. (b) F. Neese, *Coord. Chem. Rev.* 2009, **252**, 526.

28 (a) The ORCA basis set 'CoreProp' was used. This basis is based on the TurboMole DZ bases developed by Ahlrichs and coworkers and obtained brom the basis set library under ftp.chemie.uni-karlsruhe.de/pub/basen. (b) The Ahlrichs (2d2fg,3p2df) polarization functions were obtained from the Turbomole basis set library under ftp.chemie.uni-karlsruhe.de/pub/basen Sc-Zn: 2p functions from J. Wachters, *Chem. Phys.* 1970, **52**, 1033 plus one f-function from the TurboMole library.

29 A. Schäfer, H. Horn and R. Ahlrichs, *J. Chem. Phys.* 1992, **97**, 2571.

30 The Ahlrichs auxiliary basis sets were obtained from the TurboMole basis set library under ftp.chemie.uni-karlsruhe.de/pub/jbasen H-Ba; Hf-At: (a) K. Eichkorn, O. Treutler, H. Ohm, M. Haser and R. Ahlrichs, *Chem. Phys. Lett.* 1995, **240**, 283. (b) K. Eichkorn, F. Weigend, O. Treutler and R. Ahlrichs, *Theor. Chem. Acc.* 1997, **97**, 119.

31 S. C. Bart, K. Chlopek, E. Bill, M. W. Bouwkamp, E. Lobkovsky, F. Neese, K. Wieghardt and P. J. Chirik, *J. Am. Chem. Soc.* 2006, **128**, 13901.

32 K. L. Fillman, E. A. Bielinski, T. J. Schmeier, J. C. Nesvet, T. M. Woodruff, C. J. Pan, M. K. Takase, N. Hazari and M. L. Neidig, *Inorg. Chem.* 2014, **53**, 6066.

33 C. Holzhacker, M. J. Calhorda, A. Gil, M. D. Carvalho, L. P. Ferreira, B. Stöger, K. Mereiter, M. Weil, E. Pittenauer, G. Allmaier, D. Müller, P. Weinberger and K. Kirchner, *Dalton Trans.* 2014, **43**, 11152.

For Table of contents use only

Synthesis and Reactivity of Taddol-Based Chiral Fe(II) PNP Pincer Complexes – Solution Equilibria between κ^2*P,N*- and κ^3*P,N,P*-Bound PNP Pincer Ligands

Several Fe(II) complexes of the general formula [Fe(PNP-R,TAD)X_2] (R = *i*Pr, *t*Bu; X = Cl, Br) bearing chiral pincer ligands based on *R,R*-TADDOL (TAD) are described. In solution the PNP-R,TAD ligand is hemilabile and complexes with κ^2*P,N*- and κ^3*P,N,P*-bound PNP ligands are present.